


RESEARCH ARTICLE

Open Access



# Impact of topographic change on the East Asian monsoon in Japan and Eastern Asia during the Last Glacial Maximum

Evan James Gowan<sup>1\*</sup> , Tomohiko Tomita<sup>1\*</sup>, Daiki Nishioka<sup>1</sup>, Xu Zhang<sup>2,3</sup>, Yong Sun<sup>3</sup>, Xiaoxu Shi<sup>4,5</sup>, Gregor Knorr<sup>5</sup>, Uta Krebs-Kanzow<sup>5</sup>, Paul Gierz<sup>5</sup>, Gerrit Lohmann<sup>5,6</sup>, Takashi Obase<sup>7,8</sup>, Yuta Kuniyoshi<sup>7</sup> and Ayako Abe-Ouchi<sup>7</sup>

## Abstract

The rainfall patterns in Eastern Asia are largely a consequence of the Asian winter and summer monsoons. On time-scales  $10^4$ – $10^6$  of years, the position and strength of the monsoons change as a result of variations in Northern Hemisphere summer insolation. However, locally, it is possible there is a superimposed signal due to sea level change. Due to the growth of ice sheets, primarily in northern North America and Europe, global average sea level fell about 120 m during the Last Glacial Maximum (27,000–19,500 years ago). This caused the broad shallow continental shelf regions in coastal Eastern Asia to be exposed, and also greatly limited the flow of warm Pacific water into the Sea of Japan. In this study, we perform climate modelling experiments to isolate the impact of the lower sea level on the rainfall patterns in Eastern Asia. We find that the lowered sea level locally increases the summer precipitation, impacting the southern parts of Japan as well as Eastern China. The lower sea level also causes a decrease in winter precipitation in Japan. Our oxygen isotope modelling results show that the lower sea level alone is sufficient to explain the extremely depleted  $\delta^{18}\text{O}$  values measured from proxies in Last Glacial Maximum sediments in the Sea of Japan. These results show that the rainfall proxy records in the coastal Eastern Asia region, especially near the East China Sea, should not be interpreted as purely due to insolation driven changes to the monsoon front, as they also contain a local signal due to sea level changes. Further impacts of sea level changes on continental proxy records are likely limited, and they are measuring a purely global climate change signal.

**Keywords** Last Glacial Maximum, East Asian monsoon, Sea level change,  $\delta^{18}\text{O}$

## \*Correspondence:

Evan James Gowan  
evangowan@gmail.com  
Tomohiko Tomita

t-tomita@kumamoto-u.ac.jp

<sup>1</sup> Department of Earth and Environmental Sciences, Kumamoto University, 2-39-1 Kurokami Chuo-Ku, Kumamoto 860-8555, Japan

<sup>2</sup> British Antarctic Survey, Cambridge CB3 0ET, UK

<sup>3</sup> State Key Laboratory of Tibetan Plateau Earth System, Resources and Environment (TPESRE), Chinese Academy of Sciences (CAS), Beijing, China

<sup>4</sup> Southern Marine Science and Engineering Guangdong Laboratory, Zhuhai, China

<sup>5</sup> Alfred Wegener Institute, Bremerhaven, Germany

<sup>6</sup> University of Bremen, Bremen, Germany

<sup>7</sup> University of Tokyo, Tokyo, Japan

<sup>8</sup> Japan Agency for Marine-Earth Science and Technology, Yokosuka, Japan



© The Author(s) 2025. **Open Access** This article is licensed under a Creative Commons Attribution 4.0 International License, which permits use, sharing, adaptation, distribution and reproduction in any medium or format, as long as you give appropriate credit to the original author(s) and the source, provide a link to the Creative Commons licence, and indicate if changes were made. The images or other third party material in this article are included in the article's Creative Commons licence, unless indicated otherwise in a credit line to the material. If material is not included in the article's Creative Commons licence and your intended use is not permitted by statutory regulation or exceeds the permitted use, you will need to obtain permission directly from the copyright holder. To view a copy of this licence, visit <http://creativecommons.org/licenses/by/4.0/>.

## 1 Introduction

East Asia is a region extending near the boundary between the Eurasian Continent and the Pacific Ocean. This continent and the ocean form a climate peculiar to East Asia, that is, the East Asian monsoon. The East Asian summer monsoon is characterized by southerly winds between the subtropical Pacific high and the large-scale thermal low formed over the Eurasian continent, while the East Asian winter monsoon is characterized by northerly winds due to the Siberian high and the Aleutian low. The East Asian summer monsoon, along with the Indian monsoon and the Southeast Asian monsoon, brings a rainy season to this region. Thus, the East Asian monsoon is a result of global scale climate, and its changes are of critical importance in diagnosing global climate change. On the scale of thousands of years, the position and strength of the monsoon are affected by solar radiative forcing, North Atlantic Ocean conditions, and global topographic changes due to the formation of continental ice sheets (Sun et al. 2015; Liu et al. 2020; Gao et al. 2020). Shifts in the monsoon front have also impacted human civilizations (Chen et al. 2020).

The Last Glacial Maximum (LGM, 26–19.5 ka, Clark et al. (2009)) was the culmination of the last glacial cycle when continental ice sheets reached their maximum. The respective increase in CO<sub>2</sub> between the LGM and the Preindustrial and Preindustrial to present are similar in magnitude. Therefore, it is instructive to compare the changes in the monsoon between the LGM and Preindustrial to examine how large changes in radiative forcing can affect it. However, to qualitatively assess the changes in monsoon due to global climate changes, local effects like topography changes also need to be investigated and accounted for.

The climate of the LGM has been one of the focuses of the Paleoclimate Intercomparison Project (PMIP), as a way to test climate models at a time when the Earth's climate was radically different than present (Kageyama et al. 2017). Globally, temperatures were lower due to overall reductions in atmospheric CO<sub>2</sub> concentrations, reduced northern hemisphere summer insolation, and the growth of large continental ice sheets. These changes caused a weakening of the East Asian monsoons, and caused continental regions to be drier (Gao et al. 2020). Overall, the climate during the LGM is simulated to be generally drier in mainland Eastern Asia, as a result of global scale shifts in circulation patterns due to North American ice sheet albedo (Yanase and Abe-Ouchi 2007, 2010). The calculated precipitation in many of the PMIP models exhibit an anomaly in the summer precipitation in the easternmost parts of Asia, specifically in the East China Sea and around western Japan (see the supplementary materials, and Gao et al. (2020)). The main hypothesis of this

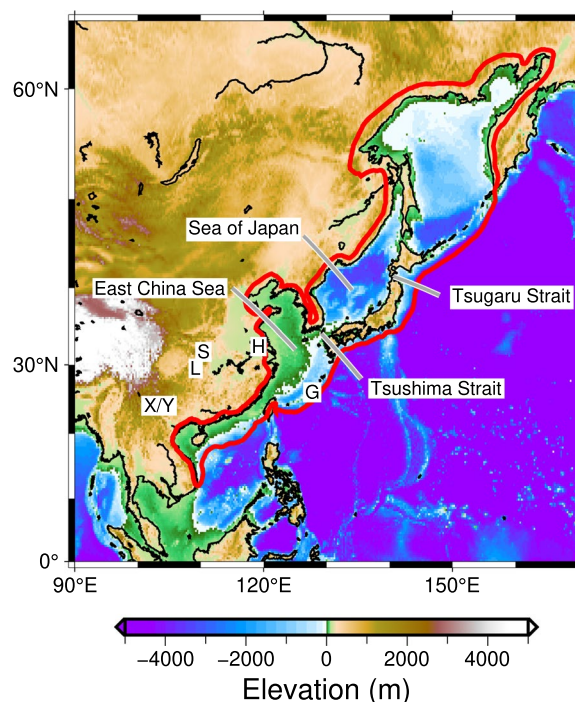


**Fig. 1** Map showing the paleotopography of Eastern Asia at the Last Glacial Maximum (20 ka) (Gowan et al. 2021), and several of the locations mentioned in the text. Green areas show places with exposed land that is within 150 m of sea level. The black outline is the modern shoreline. The red outline shows the area where the topography from the LGM was inserted into the in the preindustrial iCESM climate modelling experiments to test the impact topography change due to the sea level lowering on the climate. Areas outside of the red outline use modern topography in the experiments. The location caves with speleothem records mentioned in the text are indicated: X—Xiaobailong, S—Sanbao, H—Hulu, Y—Yangzi, L—Luoshui, G—Gyokusen

feature is that it is unrelated to global climatic factors, and is related to the drop in global sea level (e.g. Sun et al. 2021), but this has never been qualified with targeted experiments.

During the Last Glacial Maximum, global average sea level lowered by at least 115 m (Yokoyama et al. 2018; Gowan et al. 2021). In the vicinity of Japan, lowered sea level due to the growth of the ice sheets had two major impacts. The first is that it caused a near complete subaerial exposure of the East China Sea (Fig. 1). The second is that the effective closure of the Tsushima Strait prevented the inflow of warm Pacific Ocean water into the Sea of Japan. These two factors changed the local surface temperature conditions, which in turn would affect precipitation patterns (Sun et al. 2021). In this study, we are interested to evaluate the impact of the drop in sea level on the precipitation patterns in eastern Asia. Our study focuses on the impact of sea level change in the absence of other changes in the Earth system.

To investigate this, we compare the results of idealized climate modelling experiments using the isotope enabled iCESM 1.2 model that adjust a preindustrial climate simulation with modified topography in Eastern Asia and another with the addition of lower CO<sub>2</sub> levels. This allows us to distinguish the impacts of these two factors in isolation from other major changes in the climate system induced by the growth of ice sheets (which were already investigated in detail by Sun et al. (2021)) and changes in the Earth's axis of rotation. We compare the results in January and July to assess the impacts of the topography changes to winter and summer climate. The use of isotopes allows us to compare against geological proxies of climate changes. These idealized experiments indicate that the LGM climate in Eastern Asia was affected by both global scale and local factors.

## 2 The LGM in Eastern Asia

### 2.1 Modifications of topography

The growth of continental ice sheets caused global average sea level to lower by between 115 and 135 m below present during the LGM (Gowan et al. 2021; Yokoyama et al. 2000; Peltier et al. 2015). Around Eastern Asia, this had a consequence of exposing the broad continental shelf, and isolating the Sea of Japan from Pacific inflow (Fig. 1). The LGM coastline of mainland Asia extended far to the east of where it is currently (Saito 1998), and the portion of the East China Sea that covers the continental shelf was subaerially exposed. At present, the main entrances of Pacific water into the Sea of Japan are the Tsushima Strait, located between Kyushu Island in Japan and South Korea, and Tsugaru Strait, which is between Hokkaido and Honshu Island in Japan. During the LGM, the Tsushima Strait was a narrow channel with a throughflow about 95% less than present (Park et al. 2000). The strait was sufficiently wide and deep to serve as a geographical barrier for the migration of animals into Japan during the LGM (Kawamura 2007). The Tsugaru Strait remained open through the LGM, as evident by the limited migration of animals from Hokkaido to Honshu Island (Kawamura 2007), though narrower and also greatly reduced in throughflow (Koizumi et al. 2006).

### 2.2 Oxygen isotope proxies

The oxygen isotope proxies from foraminifera in ocean sediment cores and from speleothems record fluctuations in the precipitation of the East Asian monsoons. The proxies are a measure the relative difference in the fraction of <sup>18</sup>O and <sup>16</sup>O to a standard, denoted as  $\delta^{18}\text{O}$ . The  $\delta^{18}\text{O}$  values in speleothems are related to the temperature of the cave where the speleothem grows, and the  $\delta^{18}\text{O}$  value of the precipitation-derived drip water (Lachniet 2009). The water  $\delta^{18}\text{O}$  depends on the values from

the source reservoir of the precipitation, the distance from the precipitation source, the temperature of the air mass and altitude (Lachniet 2009). In Eastern Asia speleothem records, depleted  $\delta^{18}\text{O}$  values are considered to correlate with a weaker summer monsoon (Wang et al. 2008). The fluctuations of  $\delta^{18}\text{O}$  are intimately linked to changes in Northern Hemisphere summer insolation (Wang et al. 2008), with secondary signals superimposed that are related to North Atlantic climatic events (Cai et al. 2015). The  $\delta^{18}\text{O}$  values in foraminifera are dependent on the foraminifera species, water temperature, and the latent seawater  $\delta^{18}\text{O}$  (Pearson 2012). Global ocean water  $\delta^{18}\text{O}$  changes due to the growth and retreat of continental ice sheets (since  $\delta^{18}\text{O}$  is depleted in precipitation), so when ice sheets are large, there is an increase in  $\delta^{18}\text{O}$  in the ocean. During the LGM, the increase in seawater  $\delta^{18}\text{O}$  due to the growth of ice sheets is estimated to be 1‰ (Duplessy et al. 2002). We subtract this value to facilitate comparing the LGM and Holocene proxy values. Decreasing the ocean temperature also causes an increase in  $\delta^{18}\text{O}$  in foraminifera records. This is not accounted for in our comparison, so the anomalies in the data will reflect a combination of changes in latent seawater  $\delta^{18}\text{O}$  and the impacts of temperature changes.

Oxygen isotope data from planktic foraminifera were retrieved from data files included with the original studies, or in the NOAA National Centers for Environmental Information (NCEI). In some cases, we had to digitize the data from plots in the papers. The original age model was used for the proxy records if it was included. If an age model was not included, it was calculated using the OxCal P\_Sequence function (Bronk 2008; Bronk Ramsey 2009).

The isotope data from speleothems from Japan and eastern China were largely derived from the SISAL version 2.0 database (Atsawaranunt et al. 2018; Comas-Bru et al. 2020). A few additional recently published records were also included. For data derived from the SISAL database, there are a number of age models. We used the BChron-derived age model when available (Haslett and Parnell 2008), otherwise we use the linear interpolation age model. The choice to use the BChron model is because it was available for most of the speleothem records.

Oxygen isotope records for speleothems and planktonic foraminifera from ocean sediment cores are shown on Fig. 2. The location and averages for speleothems are shown on Table 1 and planktic foraminifera on Table 2. For the purposes of our analysis, we included a record if it had data in the target time ranges that we regard as representing the Holocene and LGM. For the Holocene, the range is between 0 and 7 ka (i.e. after the majority of the ice sheets had retreated to present levels and sea level

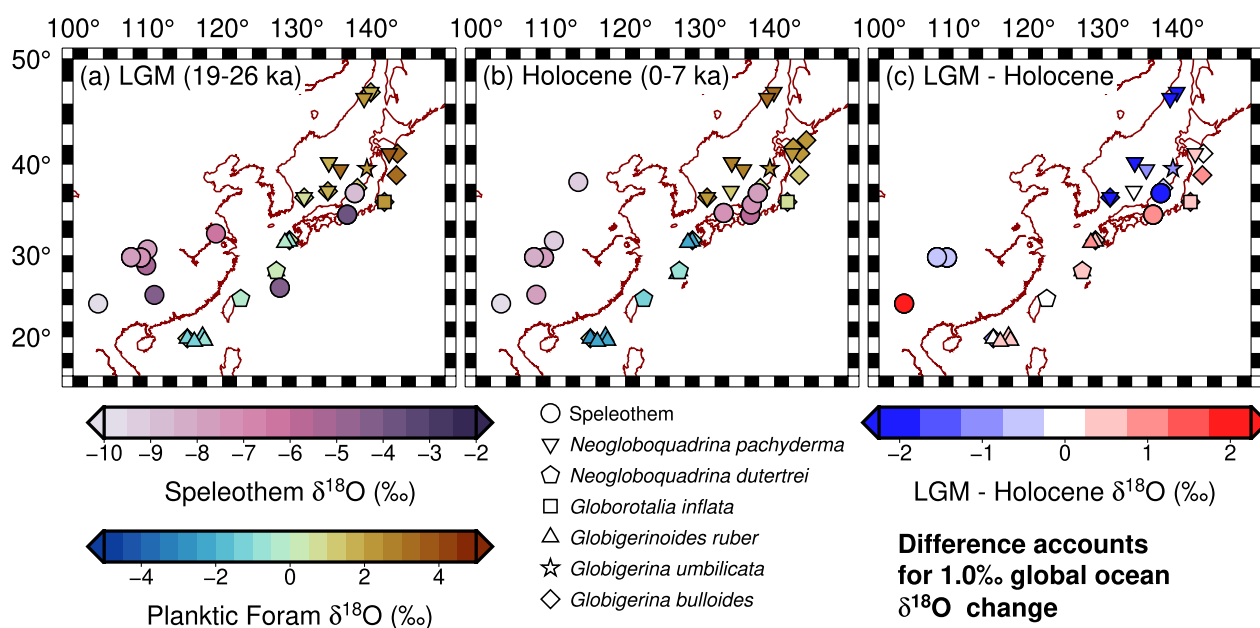


**Fig. 2**  $\delta^{18}\text{O}$  proxy records, including speleothems and planktonic foraminifera, from Eastern Asia that includes LGM and late Holocene data.  $\delta^{18}\text{O}$  values are relative to PDB or VPDB standards. The impact of the average difference in global sea water  $\delta^{18}\text{O}$ , which is approximately 1‰ (Duplessy et al. 2002), has been removed in order to assess the local changes. The source of the data can be found on Tables 1 and 2. **a** Holocene, **b** LGM, **c** Difference between records that have both Holocene and LGM values

stabilized) and 19–26 ka for the LGM (the time defined by Clark et al. (2009)). We acknowledge that this smooths some of the variability within these time periods, but regard it as a first order way to estimate the difference in  $\delta^{18}\text{O}$  between the two periods.

In terms of the anomaly (LGM–PI) patterns in these records, data from the Pacific side of Japan show a general increase in  $\delta^{18}\text{O}$  values, while the Sea of Japan has generally lower values. The two records in the Ryukyu Islands and north of Taiwan do not show any changes after removing the signal from the ice sheets. The records from the northern South China Sea show a slight increase in  $\delta^{18}\text{O}$ . The speleothems in central China have a slightly lower  $\delta^{18}\text{O}$  value, while the one in southern China has a greater  $\delta^{18}\text{O}$ . The Gyokusen cave in Okinawa does not have a Holocene record, but the modern speleothem  $\delta^{18}\text{O}$  values are 1.4–2.4‰ lower than the LGM values (Uemura et al. 2016; Asami et al. 2021). If these values are comparable to the Holocene, this would indicate a positive anomaly during the LGM.

### 2.3 Other proxies for precipitation

Although  $\delta^{18}\text{O}$  proxies are a common way to evaluate changes to the Asian monsoons, these records are still sparse in terrestrial Japan and the Korean Peninsula, which are closest to the East China Sea shelf. Here, we highlight some records that provide information on the LGM precipitation in this area. Jo et al. (2014) provided

records of the timing of speleothem growth in the Korean Peninsula. The lack of speleothems dating to the LGM implies potentially drier conditions. In contrast, the paleoenvironmental reconstructions of the LGM by U et al (2023) indicate the central Korean Peninsula maintained a relatively wet environment that could sustain wetlands and diverse fauna. Iwamoto and Inouchi (2007) analysed total carbon in a sediment core from Lake Biwa in central Japan, which reflects productivity in the lake due to influx of nutrients into the lake during the summer monsoon. This record implies that the summer monsoon was at its strongest in the late Holocene and was relatively weaker in the last glacial period, though not necessarily weakest during the LGM. Kuwae et al. (2004) investigated diatoms in Lake Biwa and also concluded that precipitation was lower relative to the late Holocene during the LGM. Gallagher et al. (2018) investigated the colours of IODP core U1427, located near the coast of Japan in the eastern Sea of Japan, and found that in the LGM, the winter monsoon dominated, while in the Holocene the summer monsoon dominated. Their result indicates that this is controlled in part by the influence of depth of the Tsushima Strait. Vats et al. (2020) performed principle component analysis on foraminifera species abundance from IODP core U1429, located southwest of Kyushu. They concluded that the summer monsoon remained strong during the LGM. Zhao et al. (2018) investigated the sediment provenance from U1429, and

concluded there was reduced precipitation in Kyushu during the LGM, but that precipitation levels were possibly higher than present on the exposed East China Sea shelf.

### 3 Climate modelling methodology

#### 3.1 Modifications of topography due to lower sea level

The experiments use a preexisting preindustrial climate model simulation with present-day topography, with the exception of the topography in Eastern Asia modified to be the same as in LGM from PaleMIST (Fig. 1). The land–sea distribution in this region is the same as in the 20 ka time slice in PaleMIST (Gowan et al. 2021). The characteristics of the modifications to Eastern Asia topography are as follows. The shelf regions with bathymetry  $> -130$  m between Vietnam and the Okhotsk Sea are exposed. The models require a connection between the Sea of Japan and the Pacific Ocean. This connection is set to be at the Tsugaru Strait between Hokkaido and Honshu, while the Tsushima Strait between Japan and South Korea is set to be closed in the experiment.

#### 3.2 iCESM

The climate modelling experiments were done with the isotope enabled version of CESM, iCESM. We used the Community Earth System Model version 1.2, iCESM (Brady et al. 2019). iCESM tracks isotopes of water (isotope tracing), including  $^{16}\text{O}$  and  $^{18}\text{O}$ , in the hydrological system, including ocean water and precipitation. From the output,  $\delta^{18}\text{O}$  can be calculated. The model uses physics based processes to determine the relative flow of the isotopes, and ensures conservation of the isotopes. This model has been evaluated against modern observations of oxygen isotopes (LeGrande and Schmidt 2006), and provides a reasonable representation of surface ocean seawater and precipitation  $\delta^{18}\text{O}$ . The resolution of the atmosphere model is  $1.9^\circ$  in latitude and  $2.5^\circ$  in longitude, and the ocean has a resolution of  $320 \times 384$ .

In order to demonstrate the role of topography changes, we have run three experiments. The first experiment (denoted as PI) is a standard preindustrial climate model simulation that has been run until it has reached equilibrium conditions (Otto-Bliesner et al. 2016). The other two experiments used this equilibrium condition as the starting point, but with the topography in the region defined in Fig. 1. In one experiment, the climate model is run for 350 model years using preindustrial climate parameters (denoted as MT, i.e. modified topography). The second experiment is run for 330 model years, but with greenhouse gas concentrations set to be the LGM values used in the PMIP4 experiments (denoted as MTCO2) (Kageyama et al. 2017). The atmospheric greenhouse gas concentrations in MTCO2 are 190 PPM

for  $\text{CO}_2$ , 375 ppb for  $\text{CH}_4$ , and 200 PPB for  $\text{N}_2\text{O}$ . The duration of these model runs is deemed long enough to adjust the ocean surface and atmosphere to investigate the changes in the land–sea mask. The evaluation of the experiments includes the average of the last 100 years of the simulations. In order to evaluate the results of topography changes, we focus on the results of January (to assess the effect on the East Asian Winter Monsoon) and July (to assess the effect on the East Asian Summer Monsoon).

Unfortunately, due to limitations on time and computing resources, we were unable to run a full LGM simulation with iCESM 1.2. However, a PMIP4 compliant LGM simulation was completed by Zhu et al. (2017). This simulation used the ICE-6G ice sheet and topography reconstruction (Peltier et al. 2015). This reconstruction is different than PaleMIST, but in Eastern Asia during the LGM, the topography changes are similar. We have compared our results with the precipitation and precipitation  $\delta^{18}\text{O}$  from this LGM simulation (denoted as LGM in our plots). Zhu et al. (2017) used a different version (iCESM 1.3) of the model. Though not the same version, they state that the results are qualitatively similar to experiments performed with iCESM 1.2 (Zhu et al. 2017).

### 4 Separating the effect of lower sea level with oxygen isotope modelling

#### 4.1 Precipitation

Figure 3 shows the January precipitation for the experiments. In the vicinity of Japan, the main change from the PI experiment in MT is a decrease in precipitation ( $1\text{--}2$  mm/day) centred over the middle of Japan. This low precipitation anomaly extends eastward to about  $160^\circ$  E. The change in precipitation in the MTCO2 experiment is not substantially different from MT in January in the study area, indicating a limited role of lower greenhouse gas concentrations in regulating the precipitation in January. The precipitation is lower in the LGM experiment compared to the PI. The MT experiment cancels much of this anomaly around the island of Honshu, while there still remains a small negative anomaly south of Kyushu and to the east of Honshu. The MTCO2 experiment further reduces the anomaly south of Kyushu. These results suggest a role of sea level fall in the winter precipitation patterns around Japan.

Figure 4 shows the July precipitation for the experiments. The MT experiment has much greater rainfall in the East China Sea and southern Japan (an anomaly of  $>2$  mm/day), indicating a large role in lowered sea level on the precipitation in this area. This does not extend into the Sea of Japan, which sees a decrease of precipitation. It seems the rain front may split into east and west bands when the East China Sea is exposed. The MTCO2

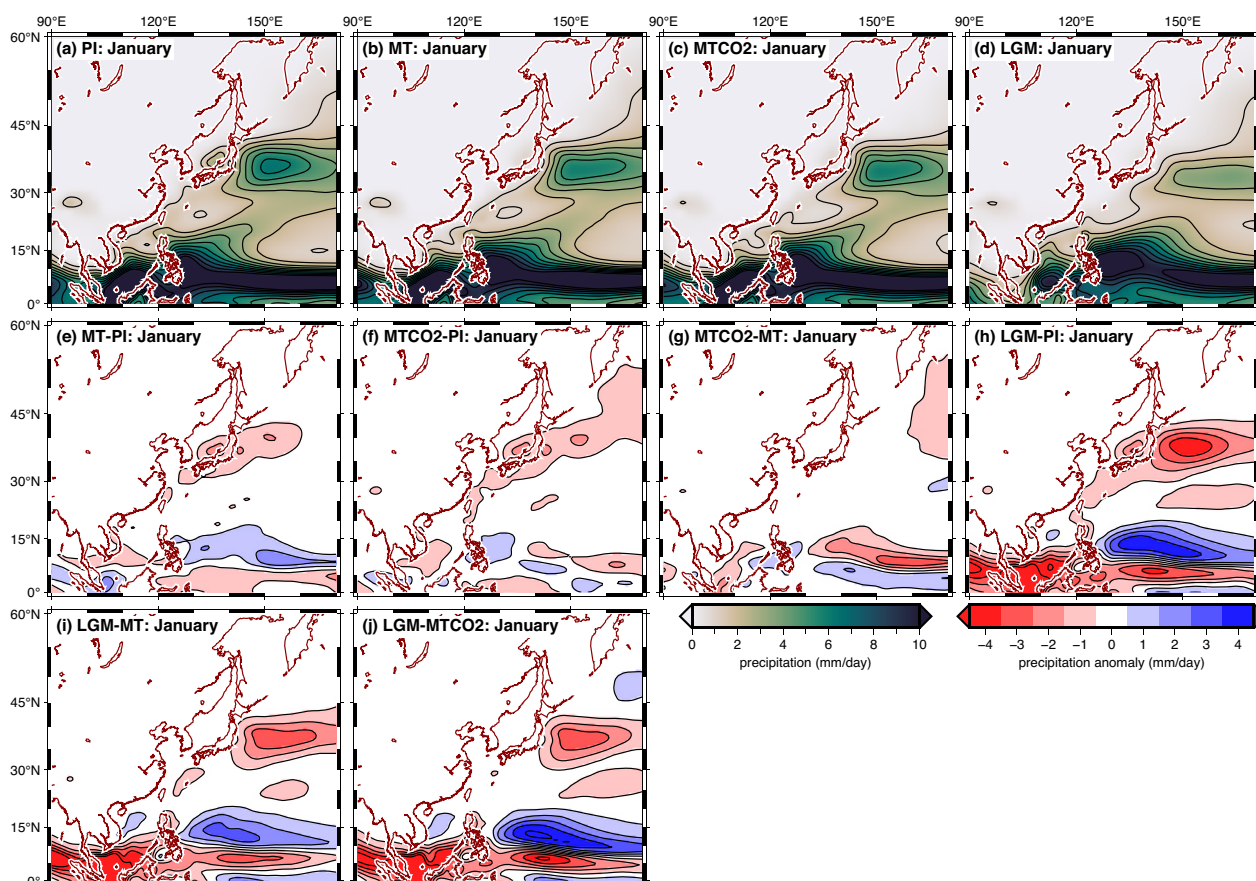


**Fig. 3** Preindustrial (PI) January precipitation and anomalies between the iCESM experiments. **a** PI precipitation, **b** Modified topography (MT) precipitation, **c** modified topography with lower CO<sub>2</sub> (MTCO2) precipitation, **d** LGM precipitation (Zhu et al. 2017), **e** MT-PI, **f** MTCO2-PI, **g** MTCO2-MT, **h** LGM-PI, **i** LGM-MT, **j** LGM-MTCO2

experiment causes precipitation near coastal East Asia to decrease (an anomaly of 1–3 mm/day), especially in the northern South China Sea. The lowered greenhouse gas concentrations does not change the overall pattern of increased precipitation in the East China Sea and southern Japan. The LGM experiment, which also includes global sea level changes, ice sheet topography, and insolation changes, also has a positive precipitation anomaly over the East China Sea, though not as high of magnitude as the MT experiment. The anomaly relative to the MTCO2 experiment is close to being the same. There is a positive precipitation anomaly (1–2 mm/day) in southeastern Asia in the LGM compared to the negative anomaly further north (e.g. northern China and central Japan), which is likely an indication of a southward shift of the summer monsoon. The precipitation changes caused by lowered sea level appears to compensate for the southward shift of the monsoon front.

#### 4.2 Temperatures

Figure 5 shows the January temperature changes for the PI, MT, and MTCO2 experiments. The exposure of the shelves in the MT experiment causes a large drop in temperatures in area around the East China Sea, as well as in the Sea of Okhotsk. This seems to also result in somewhat cooler temperatures (1–2 °C) in mainland China. The MTCO2 experiments has generally cooler temperatures everywhere, which are not amplified by the regions of shelf exposure.

Figure 6 shows the July temperature changes. The temperature anomaly in the exposed shelf in the MT experiments is the opposite of the winter, with warmer temperatures. The Sea of Japan region is 1–2 °C cooler than the PI experiment. The MTCO2 experiment also has warmer temperatures in the shelf regions compared to the PI experiment, but the generally cooler global temperatures means that it is not as pronounced as the MT experiment.

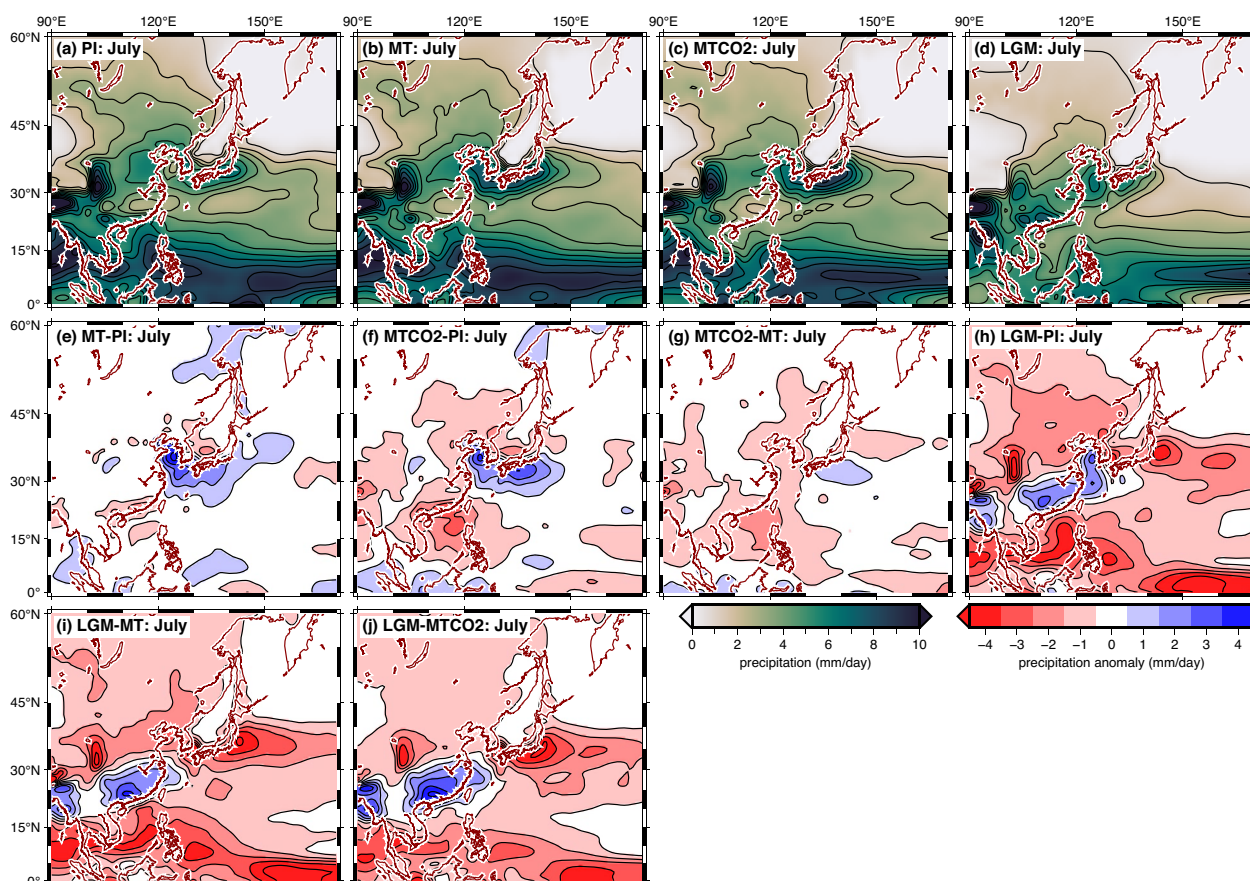


**Fig. 4** Preindustrial (PI) July precipitation and anomalies between the iCESM experiments. **a** PI precipitation, **b** Modified topography (MT) precipitation, **c** Modified topography with lower CO<sub>2</sub> (MTCO2) precipitation, **d** LGM precipitation (Zhu et al. 2017), **e** MT-PI, **f** MTCO2-PI, **g** MTCO2-MT, **h** LGM-PI, **i** LGM-MT, **j** LGM-MTCO2

### 4.3 Oxygen isotopes

Figure 7 shows the precipitation  $\delta^{18}\text{O}$  values for January. For the MT experiment, the January results show sharply lower ( $-1\text{‰}$  and lower) in areas where the topography was modified (Fig. 1). The anomaly is especially pronounced in the Sea of Japan. The MTCO2 experiment has generally lower precipitation  $\delta^{18}\text{O}$ , likely a result of overall lower surface temperatures. When the MTCO2 experiment is compared with the MT experiment, the East China Sea and Sea of Japan shows a smaller anomaly than the rest of Eastern Asia, demonstrating the dominance of sea level and topography change on the results. The LGM experiment has a slight positive anomaly in eastern China and a negative anomaly in the Sea of Japan and East China Sea regions, relative to the PI. When compared with the MT and MTCO2 experiments, the negative anomaly is not as strong in the Sea of Japan, while eastern China and the East China Sea have a much more positive ( $1\text{--}2\text{‰}$ )  $\delta^{18}\text{O}$ .

Figure 8 shows the precipitation  $\delta^{18}\text{O}$  values for July. There is a general increase ( $0.5\text{--}1.5\text{‰}$ ) in precipitation  $\delta^{18}\text{O}$  to the southeast of Japan, while there is a substantial decrease in the East China Sea and southern Sea of Japan (a decrease greater than  $-2\text{‰}$ ). This pattern persists in the MTCO2 experiment, though areas on land have a generally lower precipitation  $\delta^{18}\text{O}$  ( $-0.5\text{‰}$  and lower) likely due to lower surface temperatures. In the LGM experiment, there is a strong ( $< -2\text{‰}$ ) negative anomaly starting from the East China Sea region eastward between  $30$  and  $35^\circ\text{N}$ . The anomaly with respect to the MT experiment is reduced in the vicinity of the East China Sea and southern Sea of Japan. It is reduced even further in the MTCO2 experiment.

Figure 9 shows the near ocean surface seawater  $\delta^{18}\text{O}$  values. The ocean surface seawater  $\delta^{18}\text{O}$  in our experiments is relatively insensitive to seasonal changes, so we only show the July anomaly. The modelled PI results are consistent with observed ocean surface seawater  $\delta^{18}\text{O}$  (LeGrande and Schmidt 2006). There is a sharply negative seawater  $\delta^{18}\text{O}$  anomaly in the Sea of Japan in

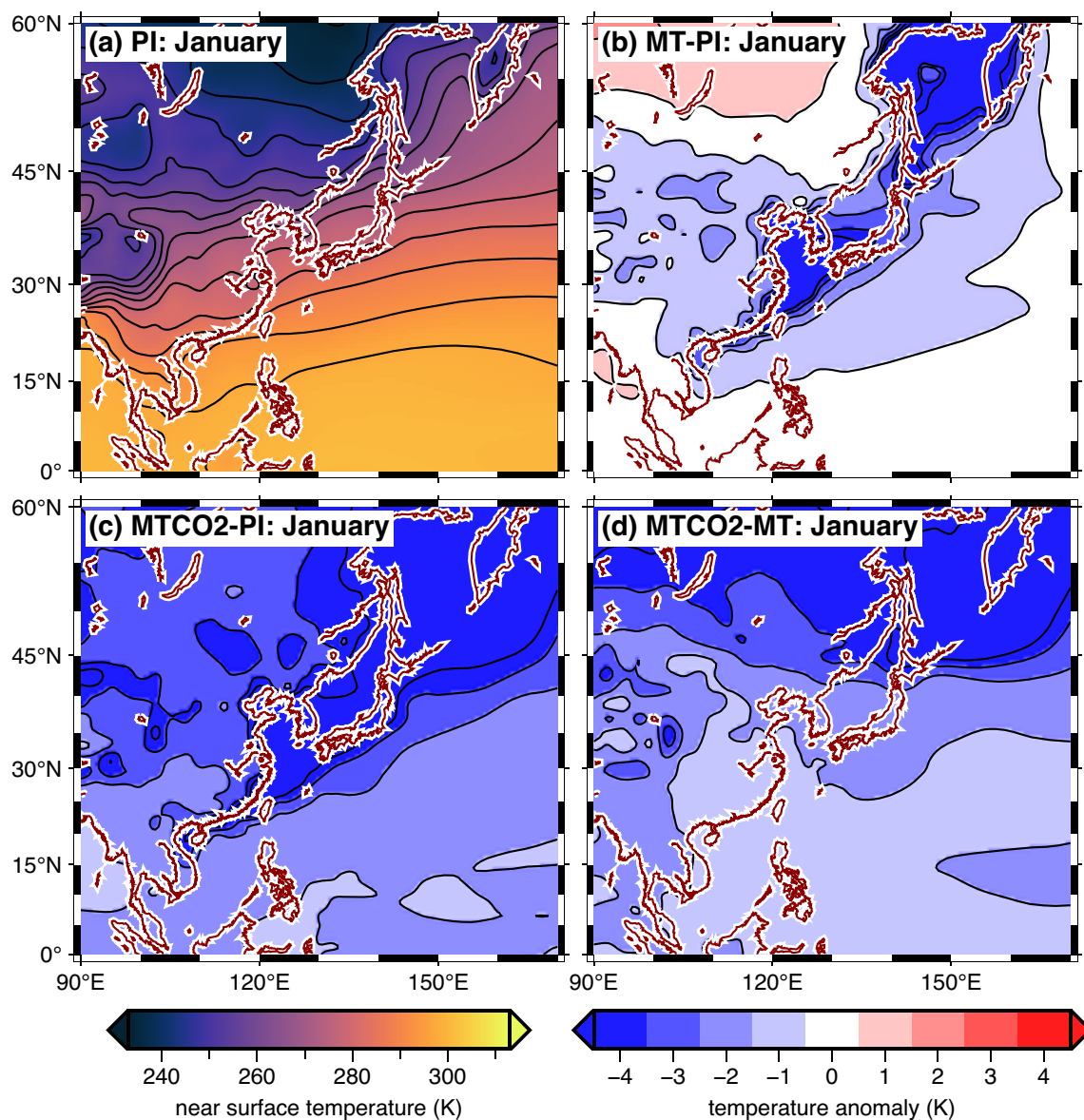


**Fig. 5** Preindustrial (PI) January near surface temperature and anomalies between the iCESM experiments. **a** PI, **b** Modified topography (MT)–PI, **c** Modified topography with lower CO<sub>2</sub> (MTCO2)–PI, **d** MTCO2–MT

the MT experiment, and a slightly negative anomaly off the coast of the East China Sea and eastern Japan. The difference between the MTCO2 and MT experiments demonstrates that this anomaly is almost entirely due to the changes in sea level. The anomaly in the Pacific can be explained by the coastline of the East China Sea moving eastward, allowing <sup>18</sup>O depleted water to reach the Pacific Ocean. The LGM experiment, after subtracting the 1‰ rise in <sup>18</sup>O due to the growth of ice sheets, displays a similar negative anomaly relative to PI in the Sea of Japan and off the coast of the East China Sea. Further negative anomalies in the North Pacific and

South China Sea are likely a consequence of other climatic impacts and ocean circulation changes during the LGM that are not captured in the MT and MTCO2 simulations.

## 5 Discussion

### 5.1 Comparison of proxies with modelled $\delta^{18}\text{O}$

To facilitate comparison, scatter plots of precipitation  $\delta^{18}\text{O}$  to speleothem and foraminifera  $\delta^{18}\text{O}$  are in supplementary Figures 7 and 8, and surface seawater  $\delta^{18}\text{O}$  to foraminifera  $\delta^{18}\text{O}$  are in supplementary Figures 9 and 10. In all plots, the LGM experiment has had 1‰ subtracted



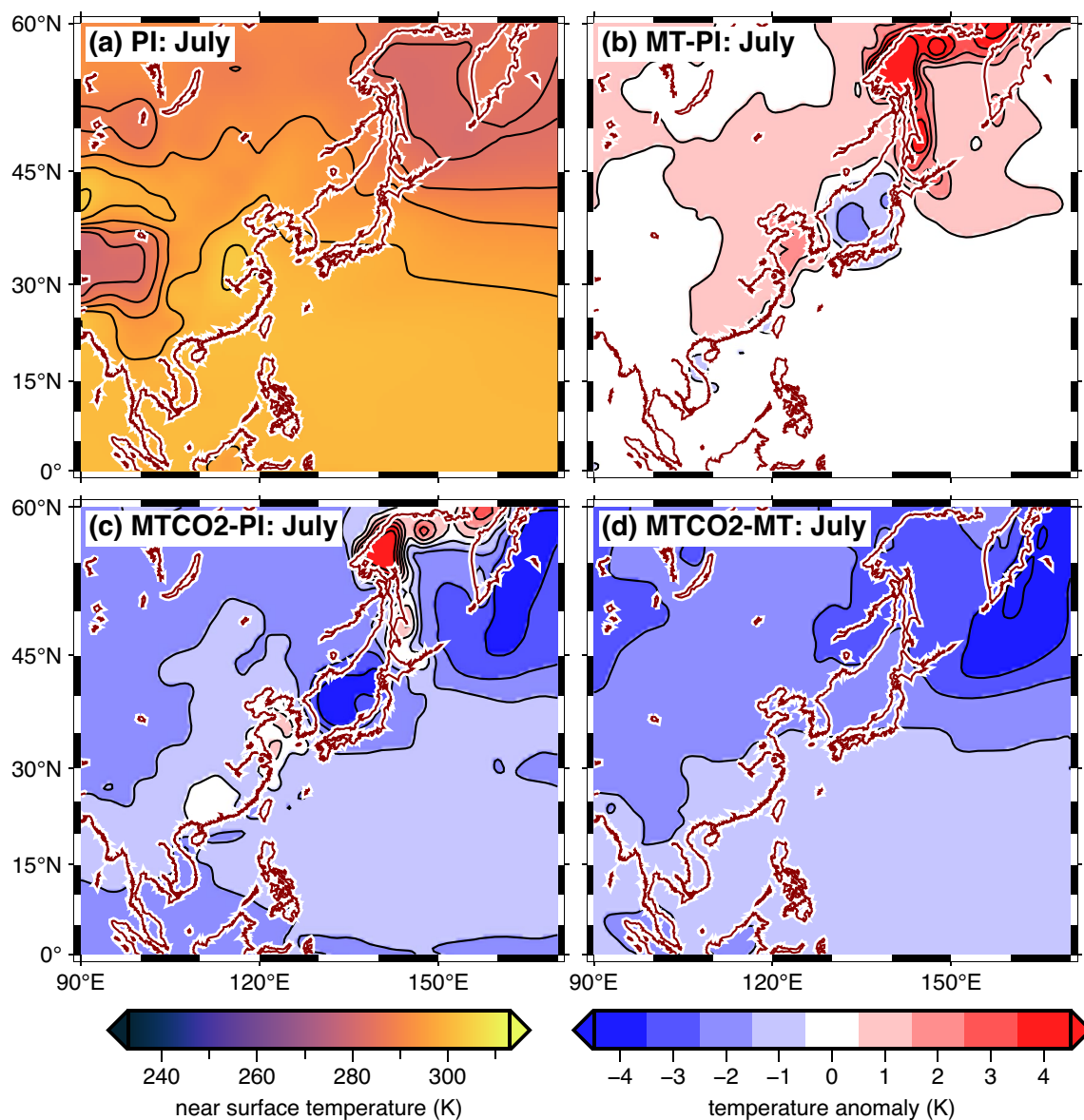


**Fig. 6** Preindustrial (PI) July near surface temperature and anomalies between the iCESM experiments. **a** PI, **b** Modified topography (MT)–PI, **c** Modified topography with lower CO<sub>2</sub> (MTCO2)–PI, **d** MTCO2–MT

to account for the changes in  $\delta^{18}\text{O}$  due to the growth of ice sheets.

In the mainland China speleothems, it is expected that a decrease in precipitation from the Asian Summer Monsoon will cause an increase in the  $\delta^{18}\text{O}$  values (Wang et al. 2008). The speleothems in Xiaobailong Cave and the combined Sanbao and Hulu records (Wang et al. 2008) indeed shows this, while the two other caves (Yangzi and Luoshui) are not as affected (Table 1). In the iCESM LGM simulation, we find an increase in  $\delta^{18}\text{O}$  in the summer precipitation with respect to PI in Eastern China south of 35°N and otherwise strongly negative values. The

modified topography experiments MT and MTCO2 indicate a complex interplay of partially opposing effects. In mainland China, we find positive  $\delta^{18}\text{O}$  anomalies in summer in the MT experiment and negative anomalies in the MTCO2 experiment. Overall, the iCESM experiments indicate that the positive  $\delta^{18}\text{O}$  found in the other caves likely requires full LGM boundary conditions (namely insolation changes and Northern Hemisphere ice sheets) to properly simulate those the observed increased  $\delta^{18}\text{O}$ , if indeed the speleothem  $\delta^{18}\text{O}$  values are a primary record of summer precipitation. The modelled January values actually more closely correspond to these data (Fig. 7).

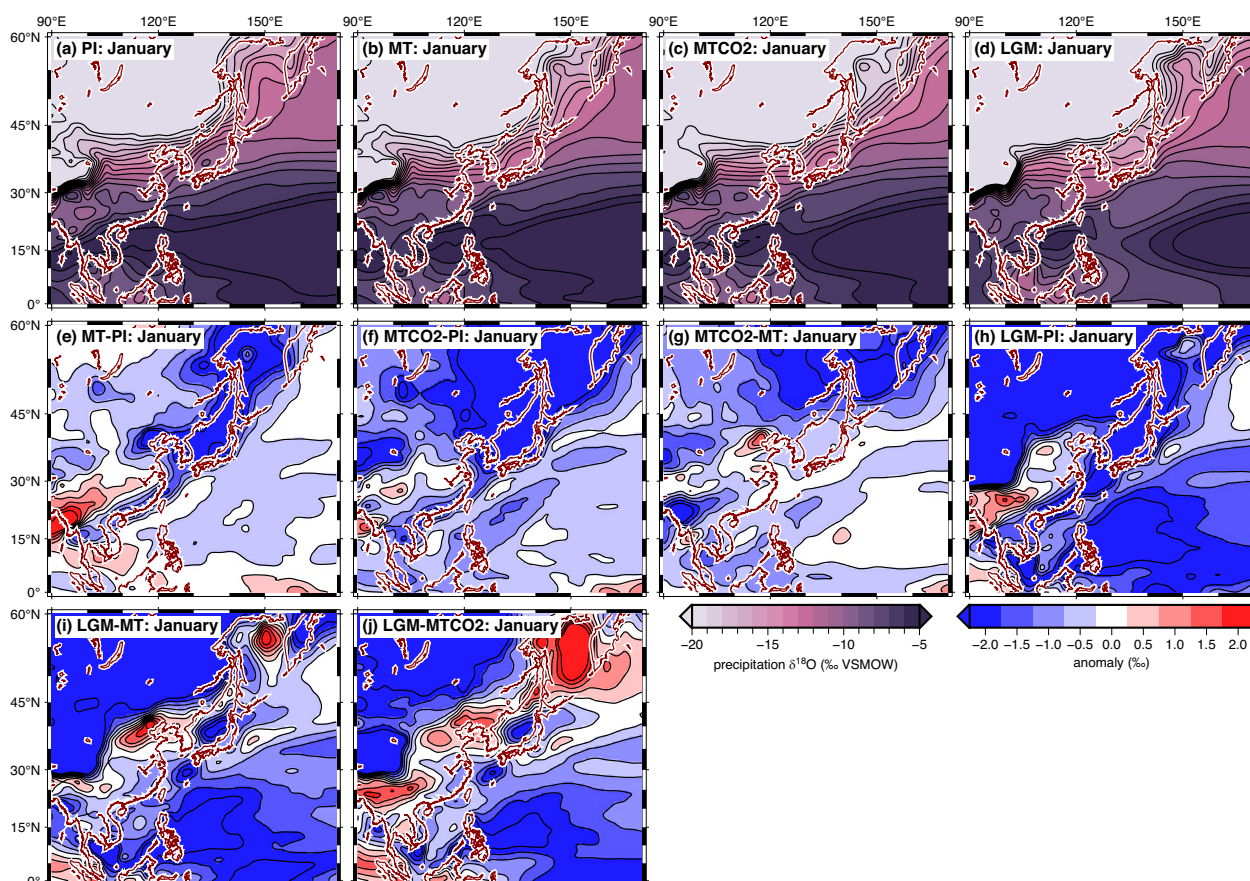


**Fig. 7** Preindustrial (PI) January precipitation  $\delta^{18}\text{O}$  and anomalies between the iCESM experiments. For the LGM experiment, 1‰ has been subtracted to account for the increase of  $\delta^{18}\text{O}$  due to the growth of ice sheets. **a** PI  $\delta^{18}\text{O}$ , **b** Modified topography (MT)  $\delta^{18}\text{O}$ , **c** Modified topography with lower  $\text{CO}_2$  (MTCO2)  $\delta^{18}\text{O}$ , **d** LGM  $\delta^{18}\text{O}$  (Zhu et al. 2017), **e** MT-PI, **f** MTCO2-PI, **g** MTCO2-MT, **h** LGM-PI, **i** LGM-MT, **j** LGM-MTCO2

All three experiments show a positive anomaly over the location Xiaobailong Cave, and zero or weakly negative anomaly in the location of the Yangzi and Luoshui caves. Only the MTCO2 experiment is unable to match the data at Xiaobailong Cave.

In Japan, there are only two speleothem records that cover both the late Holocene and LGM. The speleothem from the Sea of Japan side has a negative anomaly (Fukugaguchi cave), while the one from the Pacific Ocean side (Kiriana cave) is positive. The LGM precipitation  $\delta^{18}\text{O}$  anomaly is strongly negative ( $< -2\text{‰}$ ) at both locations, and is insensitive to season (Fig. 7h, 8h). The pattern exhibited in Japan most closely resembles the July precipitation  $\delta^{18}\text{O}$  values from the MT experiment. The record from the Sea of Japan side of Japan likely is very negative because of strong relationship with the Sea of Japan ocean surface seawater  $\delta^{18}\text{O}$  values. However, in the LGM experiment, the pattern more resembles January precipitation  $\delta^{18}\text{O}$ , which has a positive anomaly in the eastern side of Japan, and negative values on the western side (Fig. 7h). In Okinawa, there is another

speleothem record from the LGM that can, however, only be compared against modern measurements (Uemura et al. 2016; Asami et al. 2021). If the modern values are comparable to the late Holocene, this record indicates there was a positive  $\delta^{18}\text{O}$  anomaly at the LGM by as much as 1.5‰ after correcting for global ice volume. The LGM experiments have large negative anomalies in both January and July, inconsistent with this data. This value is consistent with the MT experiment July precipitation  $\delta^{18}\text{O}$  (Fig. 8e).

The planktonic foraminifera  $\delta^{18}\text{O}$  values will be affected by a number of parameters, including ocean temperature, salinity, and latent seawater  $\delta^{18}\text{O}$ , the later which will be influenced by precipitation and runoff. Our modelling results of ocean surface seawater  $\delta^{18}\text{O}$  only account for latent seawater, so care must be taken when interpreting the modelled values with the measured values from foraminifera that can be affected by the other factors. The foraminifera records in the Sea of Japan generally have a negative anomaly in the LGM, while the Pacific Ocean is positive, except the records near Taiwan and Okinawa.

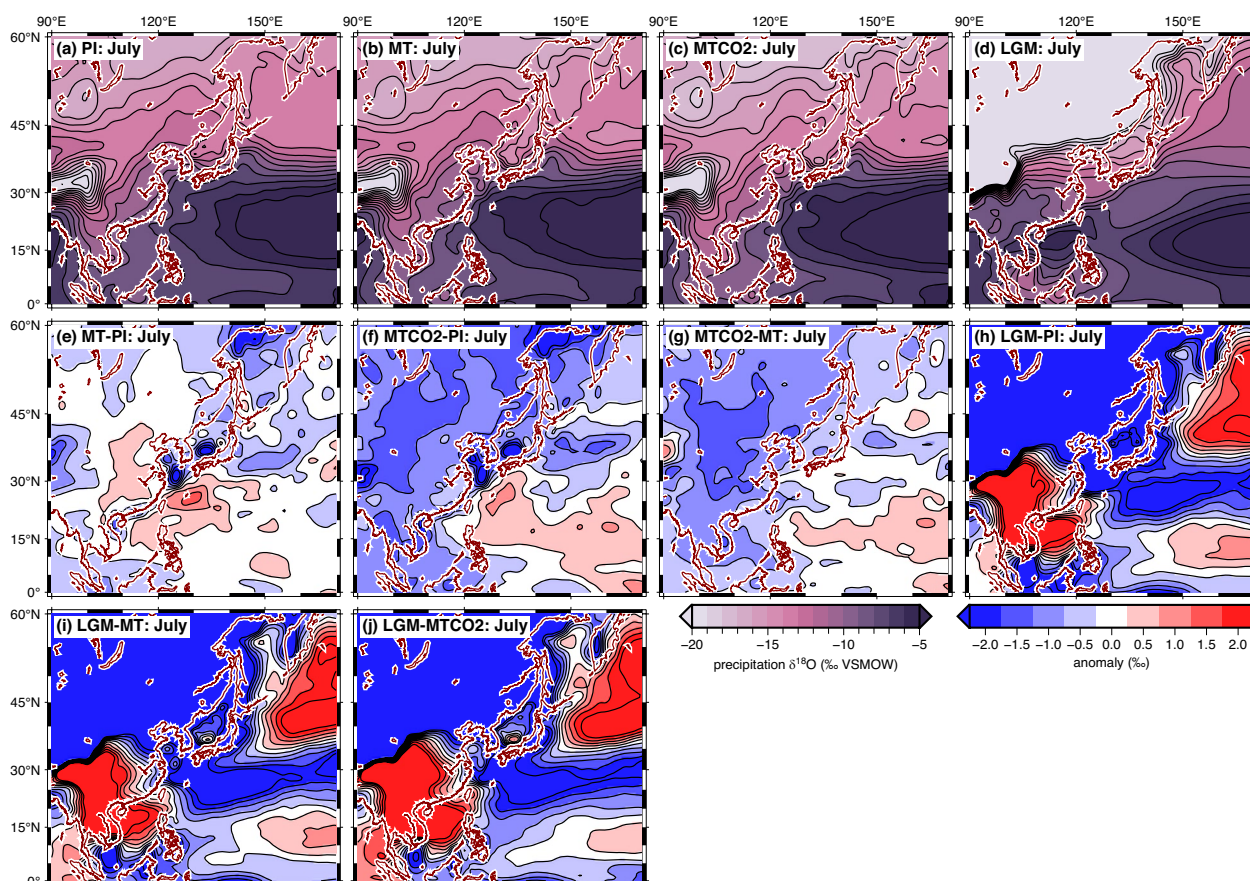


**Fig. 8** Preindustrial (PI) July precipitation  $\delta^{18}\text{O}$  and anomalies between the iCESM experiments. For the LGM experiment, 1‰ has been subtracted to account for the increase of  $\delta^{18}\text{O}$  due to the growth of ice sheets. **a** PI  $\delta^{18}\text{O}$ , **b** Modified topography (MT)  $\delta^{18}\text{O}$ , **c** Modified topography with lower  $\text{CO}_2$  (MTCO2)  $\delta^{18}\text{O}$ , **d** LGM  $\delta^{18}\text{O}$  (Zhu et al. 2017), **e** MT-PI, **f** MTCO2-PI, **g** MTCO2-MT, **h** LGM-PI, **i** LGM-MT, **j** LGM-MTCO2

Since the global ice volume is removed from these records, it should reflect a more local source for changes, or ocean temperature changes. Our modelling results confirm that the lower sea level is responsible for the sharply negative  $\delta^{18}\text{O}$  proxy values found in these records in the Sea of Japan in all three experiments (Figure. 9). This is despite the fact that lower surface temperatures may cancel part of the signal. The surface seawater  $\delta^{18}\text{O}$  has a weakly negative anomaly in the locations of the records in the South China Sea and Pacific Ocean, though these data show mostly positive to zero anomalies. The precipitation  $\delta^{18}\text{O}$  in the LGM experiment in July is positive in the South China Sea and negative elsewhere in the location of these cores. The other foraminifera records east of Eastern Asia more closely resemble the July precipitation  $\delta^{18}\text{O}$  from the MT experiment than the ocean surface seawater  $\delta^{18}\text{O}$ . This could indicate that there is a summer precipitation signal in these records, though a positive  $\delta^{18}\text{O}$  anomaly can also indicate colder water temperatures affecting the foraminifera calcite  $\delta^{18}\text{O}$ . In eastern Japan, off the coast of Honshu, the values

most closely resemble the precipitation from January in the LGM experiment. In this area, the impact of sea level change on the  $\delta^{18}\text{O}$  are likely limited.

From our results, the LGM  $\delta^{18}\text{O}$  proxy records from Eastern Asia may include a signal from precipitation changes related to lower sea level, at least in areas proximal to the exposed East China Sea and the isolated Sea of Japan. The summer monsoon on the near coastal Pacific side of East Asia is dominated by changes in topography caused by the exposure of the East China Sea and the closure of the Tsushima Strait. This causes increased precipitation in the East China Sea, South Korea, and the Pacific side of Japan (Fig. 4). The areas east of Honshu Island in Japan appear to be more related to winter precipitation, and is likely not impacted by sea level change. In the Sea of Japan and western Japan, the  $\delta^{18}\text{O}$  proxies are strongly negative, which seems mostly related to the drop in sea level that changed the seawater  $\delta^{18}\text{O}$  in the Sea of Japan (Fig. 9). The large magnitude (>2‰) anomalies in the precipitation anomaly for much of Eastern Asia in the LGM experiment make it difficult to absolutely conclude an

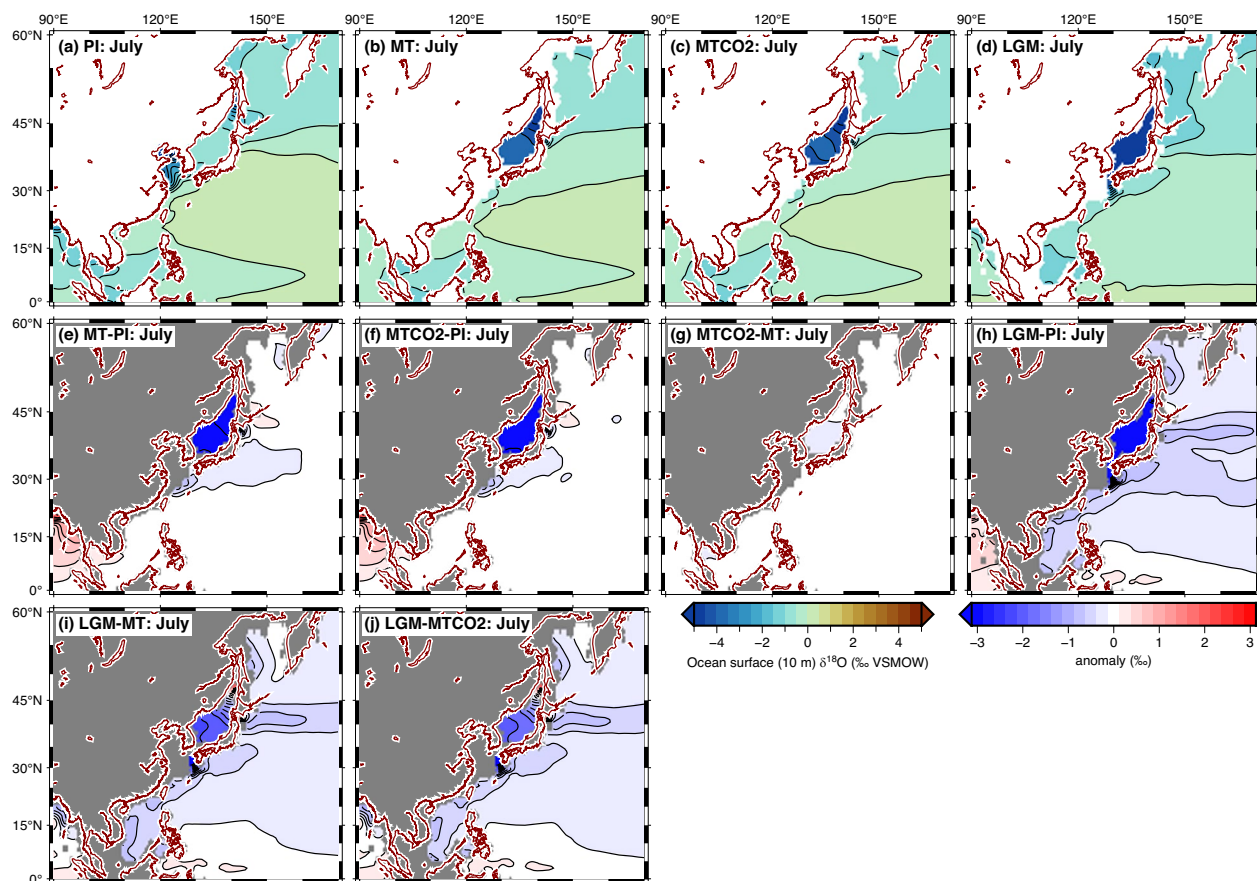


**Fig. 9** Preindustrial (PI) July near ocean surface (10 m depth)  $\delta^{18}\text{O}$  and anomalies between the iCESM experiments. For the LGM experiment, 1‰ has been subtracted to account for the increase of  $\delta^{18}\text{O}$  due to the growth of ice sheets. **a** PI  $\delta^{18}\text{O}$ , **b** Modified topography (MT)  $\delta^{18}\text{O}$ , **c** Modified topography with lower  $\text{CO}_2$  (MTCO2)  $\delta^{18}\text{O}$ , **d** LGM  $\delta^{18}\text{O}$  (Zhu et al. 2017), **e** MT–PI, **f** MTCO2–PI, **g** MTCO2–MT, **h** LGM–PI, **i** LGM–MT, **j** LGM–MTCO2

influence of sea level changes on precipitation  $\delta^{18}\text{O}$  in the mainland speleothems and Pacific coastal foraminifera records.

## 5.2 Changes in the East Asian monsoons

Long-term shifts in the East Asian Monsoons are strongly correlated to orbital forcing, namely precession. This is modulated by the cooling due to the lowering of greenhouse gases and the atmospheric effects of the ice sheet topography and albedo, and the Atlantic Meridional Overturning Circulation. More locally, as we have demonstrated, the exposure of the continental shelf and the closure of the Tsushima Strait also had an effect of shifting the summer monsoon front southwards. Since much of this precipitation anomaly is centred over what is now most of the East China Sea, there are few direct proxies of this shift in the summer monsoon front. In the winter, the model experiments show that the colder Sea of Japan would reduce the winter monsoon precipitation

in Japan. This may explain why extensive glaciers did not form in Japan during the LGM (Ono et al. 2005).

One of the main features that is likely the result of the sea level changes is that the Baiu (early summer) precipitation front appears to fork into two branches, one that is directed towards the Korean Peninsula, the other that extends along the east coast of Japan. This is possibly a combined result of warmer temperatures over the East China Sea and cooler temperatures over the Sea of Japan (Fig. 6e). The westward branch is prominent in many climate model simulations of the LGM that includes sea level changes (see the Supplementary Material). Sustained summer precipitation on the Korean Peninsula has been inferred from paleoenvironmental reconstructions (U et al. 2023). The Lake Biwa precipitation proxies (Iwamoto and Inouchi 2007; Kuwae et al. 2004) indicate generally lower precipitation, which may indicate that this area was more under the influence of the lowered precipitation regime of the Sea of Japan. No proxies exist

**Table 1** Speleothem-derived  $\delta^{18}\text{O}$  values used in this study.  $\delta^{18}\text{O}$  values are relative to PDB or VPDB standards. Uncertainties are  $1\sigma$ 

Cave name	Longitude ( $^{\circ}\text{E}$ )	Latitude ( $^{\circ}\text{N}$ )	Holocene $\delta^{18}\text{O}$ (‰)	LGM $\delta^{18}\text{O}$ (‰)	LGM–Holocene $\delta^{18}\text{O}$ (‰) <sup>1</sup>	Reference
Xiaobailong cave	103.36	24.2	$-13.9 \pm 1.1$	$-11.0 \pm 0.7$	$1.9 \pm 1.3$	Cai et al. (2015)
Yangzi cave	107.7833	29.7833	$-8.2 \pm 0.5$	$-7.6 \pm 0.4$	$-0.4 \pm 0.6$	Wu et al. (2020)
Dongge cave	108.0833	25.2833	$-7.9 \pm 0.5$	–	–	Cheng et al. (2009)
Luoshui cave	109.1167	29.7333	$-7.9 \pm 0.7$	$-7.3 \pm 0.2$	$-0.4 \pm 0.7$	Wang et al. (2022)
Yaoba Don cave	109.83	28.8	–	$-5.2 \pm 0.5$	–	Cosford et al. (2008)
Haozhu cave	109.9833	30.6833	–	$-7.8 \pm 0.2$	–	Zhang et al. (2016)
Sanbao cave	110.4333	31.667	$-9.5 \pm 0.5$	–	–	Wang et al. (2008)
Xiangshui cave	110.92	25.25	–	$-4.1 \pm 0.7$	–	Cosford et al. (2008)
Lianhua cave, Shanxi	113.7167	38.1667	$-9.5 \pm 0.6$	–	–	Dong et al. (2018)
Hulu cave	119.17	32.5	–	$-6.3 \pm 0.3$	–	Cheng et al. (2006)
Maboroshi cave	133.2166	34.8166	$-7.4 \pm 0.3$	–	–	Kato et al. (2021)
Kiriana cave	136.7666	34.6166	$-5.9 \pm 0.2$	$-3.8 \pm 0.2$	$1.1 \pm 0.3$	Mori et al. (2018)
Ohtaki cave	136.9833	35.7333	$-7.4 \pm 0.3$	–	–	Mori et al. (2018)
Fukugaguchi cave	137.7998	36.9687	$-7.6 \pm 0.3$	$-8.9 \pm 0.5$	$-2.3 \pm 0.6$	Sone et al. (2013); Amekawa et al. (2021)
Gyokusen cave	127.7492	26.1406	–	$-4.1 \pm 0.2$	–	Asami et al. (2021)

<sup>1</sup>Difference takes into account the 1‰ change in  $\delta^{18}\text{O}$  due to the volume of ice sheets at the LGM.  $\delta^{18}\text{O}$  values are relative to PDB or VPDB standards

on the eastern side of Japan can confirm the result of a southward shift in the Baiu front.

We may understand the processes that make differences in the precipitation of July in and around the East China Sea through the thermal and frictional differences between the land and sea surfaces. The occurrence of atmospheric convection would be favourable with the increased temperature of the exposed land surface than with low temperature of the sea surface. The large friction of the land surface can easily yield atmospheric convergence near the surface, which induces upward flow, compared to the small friction of the sea surface. The frictional difference is also effective in producing cyclonic circulation near the land–sea boundary of the East China Sea by the southerly winds in July.

Clemens et al. (2018), who investigated the planktic foraminifera  $\delta^{18}\text{O}$  in core U1429, located adjacent to Kyushu Island, demonstrated that it did not exhibit the expected precession paced variations like the speleothem  $\delta^{18}\text{O}$  in China. Instead, the record had a stronger obliquity (41,000 year) signal. Our results show that the larger amount of summer precipitation due to the exposure of the East China Sea shelf and/or isolation of the Sea of Japan can explain this. Since Northern Hemisphere ice sheet fluctuations are more strongly influenced by obliquity (Huybers and Wunsch 2005), it would also mean that the exposure of the shelf would also be controlled by this factor. In this case, the East Asian Summer Monsoon is only locally affected by sea

level changes (and therefore ice sheet changes), rather than the entire monsoon system. In a situation where the Northern Hemisphere summer insolation was low and ice sheets were relatively small (such as in Marine Isotope Stage (MIS) 5d, 116–109 ka), this rainfall pattern would likely not exist.

The LGM experiment shows much greater changes to precipitation patterns than the MT and MTCO2 experiments, which demonstrate that the overall position of the East Asian summer and winter monsoons is controlled by insolation and changes to Northern Hemisphere ice sheets. The increased summer precipitation anomaly in the East China Sea still exists in the LGM experiment (Fig. 4h), but the global scale climate changes reduce its amplitude compared to the MT and MTCO2 experiments. The reduction in precipitation in the area around Japan appears to be more strongly controlled by the lower sea level, and the anomaly of the LGM experiment with respect to the MTCO2 experiment is close to 0 mm/day (Fig. 3j).

In the supplementary materials, we present the January and July anomalies with respect to preindustrial from two PMIP4 compliant LGM simulations by the MIROC (Hasumi et al. 2004; Sherriff-Tadano and Abe-Ouchi 2020) and AWI-ESM (Stevens et al. 2013; Danilov et al. 2017; Scholz et al. 2019; Sidorenko et al. 2019) models using the PaleoMIST topography reconstruction. The notable difference of the setup of these models is that the AWI-ESM experiment changes the land–ocean

**Table 2** Sediment cores and marine planktic foraminifera values  $\delta^{18}\text{O}$  used in this study.  $\delta^{18}\text{O}$  values are relative to PDB or VPDB standards. Uncertainties are  $1\sigma$ 

Core name	Longitude (°E)	Latitude (°N)	Species	Holocene $\delta^{18}\text{O}$ (‰)	LGM $\delta^{18}\text{O}$ (‰)	LGM–Holocene $\delta^{18}\text{O}$ (‰) <sup>1</sup>	Reference
Core 17940-1/2	117.3833	20.1167	<i>Globigerinoides ruber</i>	$-2.5 \pm 0.2$	$-1.2 \pm 0.1$	$0.3 \pm 0.2$	Wang et al. (1999)
A7	126.9783	27.82	<i>Globigerinoides ruber</i>	$-2.2 \pm 0.2$	–	–	Sun et al. (2005)
KT94-15 PC9 GH93 KI-5	139.4068	39.5727	<i>Globigerina umbilicata</i>	$2.0 \pm 0.8$	$2.1 \pm 0.6$	$-0.9 \pm 1.0$	Xu and Oda (1999)
C11, C21, C26	131	36.5	<i>Neogloboquadrina pachyderma</i>	$2.2 \pm 0.2$	$0.6 \pm 0.5$	$-2.6 \pm 0.5$	Kim et al. (2000)
C11, C21, C26	131	36.5	<i>Globigerina bulloides</i>	$2.5 \pm 0.2$	$0.6 \pm 0.5$	$-2.9 \pm 0.5$	Kim et al. (2000)
MD01-2421	141.78	36.0233	<i>Globigerina bulloides</i>	$-0.0 \pm 0.3$	$2.4 \pm 0.6$	$1.4 \pm 0.7$	Oba et al. (2006)
MD01-2421	141.78	36.0233	<i>Globorotalia inflata</i>	$0.7 \pm 0.2$	$2.3 \pm 0.3$	$0.6 \pm 0.4$	Oba et al. (2006)
U1429	128.9975	31.617333	<i>Globigerinoides ruber</i>	$-2.4 \pm 0.2$	$-0.7 \pm 0.1$	$0.7 \pm 0.2$	Clemens et al. (2018)
KT90-9, 21	144.3167	42.45	<i>Globigerina bulloides</i>	$2.4 \pm 0.2$	–	–	Oba and Murayama (2004)
KT90-9, 5	143.5167	41.1167	<i>Globigerina bulloides</i>	$2.0 \pm 0.5$	$3.2 \pm 0.3$	$0.2 \pm 0.6$	Oba and Murayama (2004)
KH94-3, LM-8	143.3667	38.8833	<i>Globigerina bulloides</i>	$1.1 \pm 0.6$	$3.0 \pm 0.3$	$0.9 \pm 0.7$	Oba and Murayama (2004)
SO204B	115.34	19.85	<i>Globigerinoides ruber</i>	$-2.6 \pm 0.2$	$-1.4 \pm 0.1$	$0.2 \pm 0.2$	Yang et al. (2020)
SO204B	115.34	19.85	<i>Globigerina bulloides</i>	$0.8 \pm 0.3$	$0.8 \pm 0.0$	$-1.0 \pm 0.3$	Yang et al. (2020)
PC-1	128.4133	31.4583	<i>Globigerinoides ruber</i>	$-2.1 \pm 0.4$	$-0.3 \pm 0.3$	$0.8 \pm 0.5$	Chang et al. (2015)
ODP 1145	117.631	19.5840	<i>Globigerinoides ruber</i>	$-2.4 \pm 0.2$	$-0.9 \pm 0.2$	$0.5 \pm 0.3$	Oppo and Sun (2005)
ODP 1146	116.2667	19.45	<i>Globigerinoides ruber</i>	$-2.5 \pm 0.1$	$-1.1 \pm 0.2$	$0.4 \pm 0.2$	Caballero-Gill et al. (2012)
PC4	142.4003	41.1183	<i>Neogloboquadrina pachyderma</i>	$2.1 \pm 0.1$	$3.5 \pm 0.1$	$0.4 \pm 0.1$	Hoshiba et al. (2006)
L23	134.31	40.19	<i>Neogloboquadrina pachyderma</i>	$3.3 \pm 0.6$	$2.0 \pm 0.5$	$-2.3 \pm 0.8$	Gorbarenko et al. (2022)
M12	138.1383	37.5348	<i>Globigerina bulloides</i>	$0.9 \pm 0.3$	$1.3 \pm 0.5$	$-0.6 \pm 0.6$	Gorbarenko et al. (2022)
J-11	134.31	40.19	<i>Neogloboquadrina pachyderma</i>	$2.9 \pm 0.2$	$1.7 \pm 0.5$	$-2.2 \pm 0.5$	Gorbarenko et al. (2022)
L3	139.9483	47.04	<i>Neogloboquadrina pachyderma</i>	$3.3 \pm 0.2$	$1.8 \pm 0.5$	$-2.5 \pm 0.5$	Gorbarenko et al. (2022)
L3	139.9483	47.04	<i>Globigerina bulloides</i>	–	$1.3 \pm 0.4$	–	Gorbarenko et al. (2022)
L33	139.05	46.48	<i>Neogloboquadrina pachyderma</i>	$3.1 \pm 0.1$	$2.1 \pm 0.3$	$-2.0 \pm 0.3$	Gorbarenko et al. (2022)
DGKS9603	127.2706	28.14781	<i>Globigerinoides ruber</i>	$-2.3 \pm 0.3$	$-0.8 \pm 0.2$	$0.5 \pm 0.4$	Li et al. (2001)
DGKS9603	127.2706	28.14781	<i>Neogloboquadrina dutertrei</i>	$-1.0 \pm 0.2$	$0.3 \pm 0.2$	$0.3 \pm 0.3$	Li et al. (2001)
KT05-9p2	135.8667	39.4667	<i>Neogloboquadrina pachyderma</i>	$2.9 \pm 0.0$	$3.0 \pm 0.0$	$-0.9 \pm 0.0$	Minoura et al. (2012)
KH82-4-14	129.035	31.74	<i>Globigerina bulloides</i>	$-0.7 \pm 0.2$	$0.9 \pm 0.2$	$0.6 \pm 0.3$	Xu and Oda (1999)

**Table 2** (continued)

CH84-14	142.55	41.7333	<i>Globigerina bulloides</i>	2.3±0.1	–	–	Kallel et al. (1988)
MD01-2407	134.1833	37.1833	<i>Neogloboquadrina pachyderma</i>	1.0±0.2	1.8±0.5	–0.2±0.5	Yokoyama et al. (2007)
MD01-2407	134.1833	37.1833	<i>Globigerina bulloides</i>	–	1.6±0.4	–	Yokoyama et al. (2007)
ODP 1202	122.5	24.8	<i>Neogloboquadrina dutertrei</i>	–1.1±0.2	–0.1±0.2	0.0±0.3	Wei et al. (2005)

Difference takes into account the 1‰ change in  $\delta^{18}\text{O}$  due to the volume of ice sheets at the LGM

geometry to account for the effects of the lower sea level, while MIROC uses the present-day ocean–land configuration (e.g. only modifying the ice sheet geometry). One of the qualitative differences between these simulations is that there is a large positive precipitation anomaly in the East China Sea in July for AWI-ESM, while MIROC does not have this. In January, the MIROC result also does not show the lower precipitation anomaly in the Sea of Japan and western Japan, while the AWI-ESM result does. These results provide support that sea level changes locally impact the precipitation during the LGM.

The implication of this change is that it may be difficult to assess the future trajectory of rainfall patterns in the Japan and coastal Eastern Asia region by comparing with the changes between the LGM and present. The changes in the past in this area were at least partially governed by sea level changes, compared to future changes that will be dominantly controlled by increased atmospheric greenhouse gas concentrations. Untangling the relative contribution of sea level induced changes and global climate changes in the proxy records from this region may not be possible.

### 5.3 Effect of CO<sub>2</sub> changes

The MTCO<sub>2</sub> experiment was intended to show if the impacts of the topography changes on the climate in Eastern Asia during the LGM could be cancelled out by globally lower temperatures due to lower atmospheric CO<sub>2</sub>. In the East China Sea region, the MTCO<sub>2</sub> experiment has lower summer temperature (Fig. 6d), and it does somewhat lower the precipitation anomaly observed there compared with the MT experiment (Fig. 4g). The MTCO<sub>2</sub> experiment has a very large negative precipitation anomaly in the South China Sea compared to the MT experiment (Fig. 4g). This appears to be due to a southeastward shift in the summer intertropical convergence zone (ITCZ). During the winter, there is no apparent difference between the MT and MTCO<sub>2</sub> experiments, showing the dominance of lowering sea level to controlling the winter monsoon regime in the area around Japan (Fig. 3g). The lack of a stronger response

in the MTCO<sub>2</sub> demonstrates that CO<sub>2</sub> change does not drive large changes in the East Asian monsoons. This is consistent with the Chinese speleothem record, which shows that the position of the East Asian Summer Monsoon is largely controlled by Northern Hemisphere insolation (Wang et al. 2008).

The precipitation  $\delta^{18}\text{O}$  in continental regions is generally decreased in both the winter and summer (Fig. 7f, 8f) in the MTCO<sub>2</sub> experiment. This is mostly due to the impact of lowered temperatures. This more than compensates for the increase in continental precipitation  $\delta^{18}\text{O}$  in the experiment when only the topography is modified (Fig. 8e). The lowered CO<sub>2</sub> has little impact in the sea surface seawater  $\delta^{18}\text{O}$  in the Sea of Japan (Fig. 9f), demonstrating the dominance of sea level impacts on the  $\delta^{18}\text{O}$  on depleting the oxygen isotopes, despite some relative decrease in precipitation in the MTCO<sub>2</sub> experiment. Although there is greatly depleted precipitation  $\delta^{18}\text{O}$  in exposed shelf regions, the continental precipitation  $\delta^{18}\text{O}$  signal is still dominated by global climatic changes.

### 5.4 Sea level changes

The oxygen isotope values in the Sea of Japan are intimately linked with sea level changes. Planktic foraminifera  $\delta^{18}\text{O}$  values decrease by 2–3‰ when sea level falls enough to prevent significant Pacific inflow into the Sea of Japan (Sagawa et al. 2018). From our results, in the absence of other external forcings, the drop in sea level is sufficient to explain the isotopic changes. The long-term proxy records in the Sea of Japan can therefore be used as a way to assess global ice volume even in the absence of strong climatic changes. As an example, the record from Sagawa et al. (2018) shows sharp light seawater oxygen isotope anomalies in the glacial periods of the LGM, and the MIS 6 (190–130 ka) and 10 (370–330 ka) glacial periods. The MIS 8 (300–240 ka) glacial period has a much smaller peak, indicating that the global ice volume was not as large. There is no anomaly during the MIS 4 (75–55 ka) glaciation, which was estimated by Gowan et al. (2021) to have a sea level equivalent (SLE) ice volume of

about 73 m (compared to the LGM estimate of 107 m). If this value is correct, it suggests that global ice volume must exceed 73 m SLE to produce the light oxygen isotope signature in the Sea of Japan. Given that the MIS 8 glaciation had a smaller anomaly than the other glaciations, it must have just barely achieved the threshold.

## 6 Conclusions

The results of our study demonstrate that the East Asian winter and summer monsoon are affected by sea level changes, even with this exclusion of other factors such as insolation, ice sheets, and greenhouse gases. Many climate model simulations of the LGM show a large summer rainfall anomaly in the East China Sea and south of Kyushu Island. This can be attributed to the exposure of the East China Sea and isolation of the Sea of Japan due to sea level fall. The oxygen isotope analysis shows that the sea level fall can also explain the  $\delta^{18}\text{O}$  values observed in planktic foraminifera in the Sea of Japan. The lower sea level also causes a decrease in winter precipitation in Japan, driven by lowered sea surface temperatures. A reduction in atmospheric  $\text{CO}_2$  concentrations reduces the impact of the exposure of East China Sea to increase the summer rainfall. An overall cooler climate caused by the reduction in  $\text{CO}_2$  causes a further reduction of summer rainfall in the northern South China Sea, likely caused by a southward shift in the summer ITCZ. For climate model simulations that do not include the sea level fall during the LGM, it is unlikely that the pattern of precipitation  $\delta^{18}\text{O}$  changes will be well represented in the coastal areas of Eastern Asia. In continental regions of Asia, the impact of sea level change is not as substantial, and the oxygen isotope proxies are likely recording a predominantly global climate change signal.

### Abbreviations

PI:	Preindustrial
LGM:	Last Glacial Maximum
EASM:	East Asian summer monsoon
ITCZ:	Intertropical convergence zone
MIS:	Marine isotope stage
ka:	Kiloannum (thousand years)

## Supplementary Information

The online version contains supplementary material available at <https://doi.org/10.1186/s40645-024-00681-4>.

Supplementary file 1

### Acknowledgements

We thank Dr. Jiang Zhu for assistance in accessing the LGM iCESM 1.3 simulation results (Zhu et al. 2017) and the Paleoclimate Working Group and computing resources from NSF and NCAR CISL. We thank two anonymous

reviewers for their comments that improved the manuscript. Figures in this paper were created with the aid of Generic Mapping Tools (Wessel et al. 2019).

### Author contributions

The original plan for this study was conceived by EJG, TT, XZ, GL, and AAO. EJG wrote the manuscript and compiled the paleoclimate data, analysed and interpreted the modelling data, along with TT and DN. XZ and YS performed the iCESM 1.2 experiments. XS, GK, UKK, PG, and GL performed the AWI-ESM experiments. TO, YK, and AAO performed the MIROC experiments.

### Funding

EJG was supported by a Japan Society for the Promotion of Science Postdoctoral Fellowship. XZ was supported by the National Key Research and Development Projects of China (2023YFF0805201). XS is supported by the Southern Marine Science and Engineering Guangdong Laboratory (Zhuhai) (grant no. SML2023SP204), the Ocean Negative Carbon Emissions (ONCE) Program, and the National Natural Science Foundation of China (NSFC) (grant no. 42206256).

### Data availability

Data used in this paper are available in the provided tables. Model data used in the figures can be requested from EJG.

### Declarations

#### Conflict of interest

There are no conflict of interest.

Received: 25 December 2023 Accepted: 28 December 2024

Published online: 26 February 2025

### References

- Amekawa S, Kashiwagi K, Hori M, Sone T, Kato H, Okumura T, Yu T-L, Shen C-C, Kano A (2021) Stalagmite evidence for East Asian winter monsoon variability and  $^{18}\text{O}$ -depleted surface water in the Japan Sea during the last glacial period. *Prog Earth Planet Sci* 8(1):18. <https://doi.org/10.1186/s40645-021-00409-8>
- Asami R, Hondo R, Uemura R, Fujita M, Yamasaki S, Shen C-C, Wu C-C, Jiang X, Takayanagi H, Shinjo R, Kano A, Iryu Y (2021) Last glacial temperature reconstructions using coupled isotopic analyses of fossil snails and stalagmites from archaeological caves in Okinawa. *Japan Sci Rep* 11(1):21922. <https://doi.org/10.1038/s41598-021-01484-z>
- Atsawawaranunt K, Comas-Bru L, Amirnezhad Mozhdehi S, Deininger M, Harrison SP, Baker A, Boyd M, Kaushal N, Ahmad SM, Ait Ibrahim Y, Arienzo M, Bajo P, Braun K, Burstyn Y, Chawchai S, Duan W, Hatvani IG, Hu J, Kern Z, Labuhn I, Lachniet M, Lechleitner FA, Lorrey A, Pérez-Mejías C, Pickering R, Scroxton N, Members SWG (2018) The SISAL database: a global resource to document oxygen and carbon isotope records from speleothems. *Earth Syst Sci Data* 10(3):1687–1713. <https://doi.org/10.5194/essd-10-1687-2018>
- Brady E, Stevenson S, Bailey D, Liu Z, Noone D, Nusbaumer J, Otto-Bliesner BL, Tabor C, Tomas R, Wong T, Zhang J, Zhu J (2019) The connected isotopic water cycle in the Community Earth System Model Version 1. *J Adv Model Earth Syst* 11(8):2547–2566. <https://doi.org/10.1029/2019MS001663>
- Bronk Ramsey C (2008) Deposition models for chronological records. *Quat Sci Rev* 27(1):42–60. <https://doi.org/10.1016/j.quascirev.2007.01.019>
- Bronk Ramsey C (2009) Bayesian analysis of radiocarbon dates. *Radiocarbon* 51(1):337–360. <https://doi.org/10.1017/S0033822200033865>
- Caballero-Gill RP, Clemens SC, Prell WL (2012) Direct correlation of Chinese speleothem  $\delta^{18}\text{O}$  and south china sea planktonic  $\delta^{18}\text{O}$ : Transferring a speleothem chronology to the benthic marine chronology. *Paleoceanography* 27(2):2203. <https://doi.org/10.1029/2011PA002268>
- Cai Y, Fung IY, Edwards RL, An Z, Cheng H, Lee J-E, Tan L, Shen C-C, Wang X, Day JA, Zhou W, Kelly MJ, Chiang JCH (2015) Variability of stalagmite-inferred Indian monsoon precipitation over the past 252,000 y. *Proc Natl Acad Sci* 112(10):2954–2959. <https://doi.org/10.1073/pnas.1424035112>



- Chang F, Li T, Xiong Z, Xu Z (2015) Evidence for sea level and monsoonally driven variations in terrigenous input to the northern East China Sea during the last 24.3 ka. *Paleoceanography* 30(6):642–658. <https://doi.org/10.1002/2014PA002733>
- Chen F, Chen S, Zhang X, Chen J, Wang X, Gowan EJ, Qiang M, Dong G, Wang Z, Li Y, Xu Q, Xu Y, Smol JP, Liu J (2020) Asian dust-storm activity dominated by Chinese dynasty changes since 2000 BP. *Nat Commun* 11(1):992. <https://doi.org/10.1038/s41467-020-14765-4>
- Cheng H, Edwards RL, Wang Y, Kong X, Ming Y, Kelly MJ, Wang X, Gallup CD, Liu W (2006) A penultimate glacial monsoon record from Hulu Cave and two-phase glacial terminations. *Geology* 34(3):217–220. <https://doi.org/10.1130/G22289.1>
- Cheng H, Fleitmann D, Edwards RL, Wang X, Cruz FW, Auler AS, Mangini A, Wang Y, Kong X, Burns SJ, Matter A (2009) Timing and structure of the 8.2 kyr B.P. event inferred from  $\delta^{18}\text{O}$  records of stalagmites from China, Oman, and Brazil. *Geology* 37(11):1007–1010. <https://doi.org/10.1130/G30126A.1>
- Clark PU, Dyke AS, Shakun JD, Carlson AE, Clark J, Wohlfarth B, Mitrovica JX, Hostetler SW, McCabe AM (2009) The last glacial maximum. *Science* 325(5941):710–714. <https://doi.org/10.1126/science.1172873>
- Clemens SC, Holbourn A, Kubota Y, Lee KE, Liu Z, Chen G, Nelson A, Fox-Kemper B (2018) Precession-band variance missing from East Asian monsoon runoff. *Nat Commun* 9(1):3364. <https://doi.org/10.1038/s41467-018-05814-0>
- Comas-Bru L, Rehfeld K, Roesch C, Amirnezhad-Mozhdehi S, Harrison SP, Atsawawanunt K, Ahmad SM, Brahim YA, Baker A, Bosomworth M, Breitenbach SFM, Burstyn Y, Columbu A, Deininger M, Demény A, Dixon B, Fohlmeister J, Hatvani IG, Hu J, Kaushal N, Kern Z, Labuhn I, Lechleitner FA, Lorrey A, Martrat B, Novello VF, Oster J, Pérez-Mejías C, Scholz D, Scroton N, Sinha N, Ward BM, Warken S, Zhang H (2020) SISALv2: a comprehensive speleothem isotope database with multiple age-depth models. *Earth Syst Sci Data* 12(4):2579–2606. <https://doi.org/10.5194/essd-12-2579-2020>
- Cosford J, Qing H, Yuan D, Zhang M, Holmden C, Patterson W, Hai C (2008) Millennial-scale variability in the Asian monsoon: evidence from oxygen isotope records from stalagmites in southeastern China. *Palaeogeogr Palaeoclimatol Palaeoecol* 266(1):3–12. <https://doi.org/10.1016/j.palaeo.2008.03.029>
- Danilov S, Sidorenko D, Wang Q, Jung T (2017) The Finite-volume Sea Ice-Ocean Model (FESOM2). *Geosci Model Dev* 10(2):765–789. <https://doi.org/10.5194/gmd-10-765-2017>
- Dong J, Shen C-C, Kong X, Wu C-C, Hu H-M, Ren H, Wang Y (2018) Rapid retreat of the East Asian summer monsoon in the middle Holocene and a millennial weak monsoon interval at 9 ka in northern China. *J Asian Earth Sci* 151:31–39. <https://doi.org/10.1016/j.jseas.2017.10.016>
- Duplessy J-C, Labeyrie L, Waelbroeck C (2002) Constraints on the ocean oxygen isotopic enrichment between the Last Glacial Maximum and the Holocene: Paleoclimatographic implications. *Quatern Sci Rev* 21(1):315–330. [https://doi.org/10.1016/S0277-3791\(01\)00107-X](https://doi.org/10.1016/S0277-3791(01)00107-X). (EPILOG)
- Gallagher SJ, Sagawa T, Henderson AC, Saavedra-Pellitero M, De Vleeschouwer D, Black H, Itaki T, Toucanne S, Bassetti M-A, Clemens S (2018) East Asian monsoon history and paleoceanography of the Japan Sea over the last 460,000 years. *Paleoceanogr Paleoclimatol* 33(7):683–702. <https://doi.org/10.1029/2018PA003331>
- Gao Y, Liu Z, Lu Z (2020) Dynamic effect of last glacial maximum ice sheet topography on the East Asian summer monsoon. *J Clim* 33(16):6929–6944. <https://doi.org/10.1175/JCLI-D-19-0562.1>
- Gorbarenko SA, Shi X, Bosin AA, Liu Y, Artemova AV, Zou J, Yanchenko EA, Vasilenko YP, Wu Y, Vladimirov AS (2022) Relative sea level changes during the Last Glacial Maximum and deglaciation (33–15 ka) inferred from the  $\delta^{18}\text{O}$  records of planktic foraminifera from the Sea of Japan. *Quatern Sci Rev* 279:107386. <https://doi.org/10.1016/j.quascirev.2022.107386>
- Gowan EJ, Zhang X, Khosravi S, Rovere A, Stocchi P, Hughes ALC, Gyllencreutz R, Mangerud J, Svendsen J, Lohmann G (2021) A new global ice sheet reconstruction for the past 80 000 years. *Nat Commun* 12:1199. <https://doi.org/10.1038/s41467-021-21469-w>
- Haslett J, Parnell A (2008) A simple monotone process with application to radiocarbon-dated depth chronologies. *J R Stat Soc Ser C Appl Stat* 57(4):399–418. <https://doi.org/10.1111/j.1467-9876.2008.00623.x>
- Hasumi H, Emori S (2004) K-1 coupled GCM (MIROC) description. K-1 Technical Report 1, University of Tokyo Center For Climate System Research. Accessed 21 Dec 2023. [https://ccsr.aori.u-tokyo.ac.jp/~hasumi/miroc\\_description.pdf](https://ccsr.aori.u-tokyo.ac.jp/~hasumi/miroc_description.pdf)
- Hoshiba M, Ahagon N, Ohkushi K, Uchida M, Motoyama I, Nishimura A (2006) Foraminiferal oxygen and carbon isotopes during the last 34 kyr off northern Japan, northwestern Pacific. *Mar Micropaleontol* 61(4):196–208. <https://doi.org/10.1016/j.marmicro.2006.07.001>
- Huybers P, Wunsch C (2005) Obliquity pacing of the late Pleistocene glacial terminations. *Nature* 434(7032):491–494. <https://doi.org/10.1038/nature03401>
- Iwamoto N, Inouchi Y (2007) Reconstruction of millennial-scale variations in the East Asian summer monsoon over the past 300 ka based on the total carbon content of sediment from Lake Biwa. *Jpn Environ Geol* 52(8):1607–1616. <https://doi.org/10.1007/s00254-006-0606-5>
- Jo K-n, Woo KS, Yi S, Yang DY, Lim HS, Wang Y, Cheng H, Edwards RL (2014) Mid-latitude interhemispheric hydrologic seesaw over the past 550,000 years. *Nature* 508(7496):378–382. <https://doi.org/10.1038/nature13076>
- Kageyama M, Albani S, Braconnot P, Harrison SP, Hopcroft PO, Ivanovic RF, Lambert F, Marti O, Peltier WR, Peterschmitt J-Y, Roche DM, Tarasov L, Zhang X, Brady EC, Haywood AM, LeGrande AN, Lunt DJ, Mahowald NM, Mikolajewicz U, Nisancioglu KH, Otto-Bliesner BL, Renssen H, Tomas RA, Zhang Q, Abe-Ouchi A, Bartlein PJ, Cao J, Li Q, Lohmann G, Ohgaito R, Shi X, Volodin E, Yoshida K, Zhang X, Zheng W (2017) The PMIP4 contribution to CMIP6 - Part 4: scientific objectives and experimental design of the PMIP4-CMIP6 Last Glacial Maximum experiments and PMIP4 sensitivity experiments. *Geosci Model Dev* 10(11):4035–4055. <https://doi.org/10.5194/gmd-10-4035-2017>
- Kallel N, Labeyrie LD, Arnold M, Okada H, Dudley WC, Duplessy JC (1988) Evidence of cooling during the younger Dryas in the western North Pacific. *Oceanol Acta* 11(4):369–375
- Kato H, Amekawa S, Hori M, Shen C-C, Kuwahara Y, Senda R, Kano A (2021) Influences of temperature and the meteoric water  $\delta^{18}\text{O}$  value on a stalagmite record in the last deglacial to middle Holocene period from southwestern Japan. *Quatern Sci Rev* 253:106746. <https://doi.org/10.1016/j.quascirev.2020.106746>
- Kawamura Y (2007) Last glacial and holocene land mammals of the Japanese islands: Their fauna, extinction and immigration. *The Quaternary Research (Daiyonki-Kenkyu)* 46(3):171–177. <https://doi.org/10.4116/jaqua.46.171>
- Kim J-M, Kennett JP, Park B-K, Kim DC, Kim GY, Roark EB (2000) Paleoclimatographic change during the last deglaciation, east sea of Korea. *Paleoceanography* 15(2):254–266. <https://doi.org/10.1029/1999PA000393>
- Koizumi I, Tada R, Narita H, Irino T, Aramaki T, Oba T, Yamamoto H (2006) Paleoclimatographic history around the Tsugaru Strait between the Japan Sea and the Northwest Pacific Ocean since 30 cal kyr BP. *Palaeogeogr Palaeoclimatol Palaeoecol* 232(1):36–52. <https://doi.org/10.1016/j.palaeo.2005.09.003>
- Kuwae M, Yoshikawa S, Tsugeki N, Inouchi Y (2004) Reconstruction of a climate record for the past 140 kyr based on diatom valve flux data from Lake Biwa. *Jpn J Paleolimnol* 32(1):19–39. <https://doi.org/10.1023/B:JOPL.0000025284.96452.26>
- Lachniet MS (2009) Climatic and environmental controls on speleothem oxygen-isotope values. *Quatern Sci Rev* 28(5):412–432. <https://doi.org/10.1016/j.quascirev.2008.10.021>
- LeGrande AN, Schmidt GA (2006) Global gridded data set of the oxygen isotopic composition in seawater. *Geophys Res Lett*. <https://doi.org/10.1029/2006GL026011>
- Li T, Liu Z, Hall MA, Berne S, Saito Y, Cang S, Cheng Z (2001) Heinrich event imprints in the Okinawa Trough: evidence from oxygen isotope and planktonic foraminifera. *Palaeogeogr Palaeoclimatol Palaeoecol* 176(1):133–146. [https://doi.org/10.1016/S0031-0182\(01\)00332-7](https://doi.org/10.1016/S0031-0182(01)00332-7)
- Liu X, Sun Y, Vandenbergh J, Cheng P, Zhang X, Gowan EJ, Lohmann G, An Z (2020) Centennial- to millennial-scale monsoon changes since the last deglaciation linked to solar activities and North Atlantic cooling. *Clim Past* 16(1):315–324. <https://doi.org/10.5194/cp-16-315-2020>
- Minoura K, Akaki K, Nemoto N, Tsukawaki S, Nakamura T (2012) Origin of deep water in the Japan Sea over the last 145kyr. *Palaeogeogr Palaeoclimatol Palaeoecol* 339–341:25–38. <https://doi.org/10.1016/j.palaeo.2012.04.011>
- Mori T, Kashiwagi K, Amekawa S, Kato H, Okumura T, Takashima C, Wu C-C, Shen C-C, Quade J, Kano A (2018) Temperature and seawater isotopic controls on two stalagmite records since 83 ka from maritime Japan. *Quatern Sci Rev* 192:47–58. <https://doi.org/10.1016/j.quascirev.2018.05.024>

- Oba T, Murayama M (2004) Sea-surface temperature and salinity changes in the northwest Pacific since the Last Glacial Maximum. *J Quat Sci* 19(4):335–346. <https://doi.org/10.1002/jqs.843>
- Oba T, Irino T, Yamamoto M, Murayama M, Takamura A, Aoki K (2006) Paleooceanographic change off central Japan since the last 144,000 years based on high-resolution oxygen and carbon isotope records. *Global Planet Change* 53(1):5–20. <https://doi.org/10.1016/j.gloplacha.2006.05.002>. **(Late Quaternary paleoceanography of the northwestern Pacific: Results from IMAGES program)**
- Ono Y, Aoki T, Hasegawa H, Dali L (2005) Mountain glaciation in Japan and Taiwan at the global Last Glacial Maximum. *Quatern Int* 138–139:79–92. <https://doi.org/10.1016/j.quaint.2005.02.007>
- Oppo DW, Sun Y (2005) Amplitude and timing of sea-surface temperature change in the northern South China Sea: dynamic link to the East Asian monsoon. *Geology* 33(10):785–788. <https://doi.org/10.1130/G21867.1>
- Otto-Bliesner BL, Brady EC, Fasullo J, Jahn A, Landrum L, Stevenson S, Rosenbloom N, Mai A, Strand G (2016) Climate variability and change since 850 CE: an ensemble approach with the Community Earth System Model. *Bull Am Meteor Soc* 97(5):735–754. <https://doi.org/10.1175/BAMS-D-14-00233.1>
- Park S-C, Yoo D-G, Lee C-W, Lee E-I (2000) Last glacial sea-level changes and paleogeography of the Korea (Tsushima) Strait. *Geo-Mar Lett* 20(2):64–71. <https://doi.org/10.1007/s003670000039>
- Pearson PN (2012) Oxygen isotopes in foraminifera: overview and historical review. *Paleontol Soc P* 18:1–38. <https://doi.org/10.1017/S108933260002539>
- Peltier WR, Argus DF, Drummond R (2015) Space geodesy constrains ice age terminal deglaciation: the global ICE-6G\_C (VM5a) model. *J Geophys Res Solid Earth* 120:450–487. <https://doi.org/10.1002/2014JB011176>
- Sagawa T, Nagahashi Y, Satoguchi Y, Holbourn A, Itaki T, Gallagher SJ, Saavedra-Pellitero M, Ikehara K, Irino T, Tada R (2018) Integrated tephrostratigraphy and stable isotope stratigraphy in the Japan Sea and East China Sea using IODP Sites U1426, U1427, and U1429, Expedition 346 Asian Monsoon. *Prog Earth Planet Sci* 5(1):18. <https://doi.org/10.1186/s40645-018-0168-7>
- Saito Y (1998) Sea levels of the Last Glacial in the East China Sea continental shelf. *The Quaternary Research (Daiyonki-Kenkyu)* 37(3):235–242. <https://doi.org/10.4116/jaqua.37.235>
- Scholz P, Sidorenko D, Gurses O, Danilov S, Koldunov N, Wang Q, Sein D, Smolentseva M, Rakowsky N, Jung T (2019) Assessment of the Finite-volume Sea ice–Ocean Model (FESOM2.0) - Part 1: description of selected key model elements and comparison to its predecessor version. *Geosci Model Dev* 12(11):4875–4899. <https://doi.org/10.5194/gmd-12-4875-2019>
- Sherriff-Tadano S, Abe-Ouchi A (2020) Roles of sea ice-surface wind feedback in maintaining the glacial Atlantic Meridional overturning circulation and climate. *J Clim* 33(8):3001–3018. <https://doi.org/10.1175/JCLI-D-19-0431.1>
- Sidorenko D, Goessling HF, Koldunov NV, Scholz P, Danilov S, Barbi D, Cabos W, Gurses O, Harig S, Hinrichs C, Juricke S, Lohmann G, Losch M, Mu L, Rackow T, Rakowsky N, Sein D, Semmler T, Shi X, Stepanek C, Streffing J, Wang Q, Wekerle C, Yang H, Jung T (2019) Evaluation of FESOM2.0 Coupled to ECHAM6.3: preindustrial and HighResMIP simulations. *J Adv Modeling Earth Syst* 11(11):3794–3815. <https://doi.org/10.1029/2019M5001696>
- Sone T, Kano A, Okumura T, Kashiwagi K, Hori M, Jiang X, Shen C-C (2013) Holocene stalagmite oxygen isotopic record from the Japan Sea side of the Japanese Islands, as a new proxy of the East Asian winter monsoon. *Quatern Sci Rev* 75:150–160. <https://doi.org/10.1016/j.quascirev.2013.06.019>
- Stevens B, Giorgetta M, Esch M, Mauritsen T, Crueger T, Rast S, Salzmann M, Schmidt H, Bader J, Block K, Brokopf R, Fast I, Kinne S, Kornblueh L, Lohmann U, Pincus R, Reichler T, Roeckner E (2013) Atmospheric component of the MPI-M earth system model: ECHAM6. *J Adv Model Earth Syst* 5(2):146–172. <https://doi.org/10.1002/jame.20015>
- Sun Y, Wu H, Kageyama M, Ramstein G, Li LZ, Tan N, Lin Y, Liu B, Zheng W, Zhang W, Zou L, Zhou T (2021) The contrasting effects of thermodynamic and dynamic processes on East Asian summer monsoon precipitation during the Last Glacial Maximum: a data-model comparison. *Clim Dyn* 56(3):1303–1316. <https://doi.org/10.1007/s00382-020-05533-7>
- Sun Y, Oppo DW, Xiang R, Liu W, Gao S (2005) Last deglaciation in the Okinawa trough: subtropical northwest Pacific link to Northern Hemisphere and tropical climate. *Paleoceanography* 20(4):4005. <https://doi.org/10.1029/2004PA001061>
- Sun Y, Kutzbach J, An Z, Clemens S, Liu Z, Liu W, Liu X, Shi Z, Zheng W, Liang L, Yan Y, Li Y (2015) Astronomical and glacial forcing of East Asian summer monsoon variability. *Quatern Sci Rev* 115:132–142. <https://doi.org/10.1016/j.quascirev.2015.03.009>
- U C, Choe RS, Ri JN, Han MG (2023) Paleoenvironment and human activity on the central Korean Peninsula during the late MIS 3 and MIS 2. *Quatern Res* 112:67–77. <https://doi.org/10.1017/qua.2022.48>
- Uemura R, Nakamoto M, Asami R, Mishima S, Gibo M, Masaka K, Jin-Ping C, Wu C-C, Chang Y-W, Shen C-C (2016) Precise oxygen and hydrogen isotope determination in nanoliter quantities of speleothem inclusion water by cavity ring-down spectroscopic techniques. *Geochim Cosmochim Acta* 172:159–176. <https://doi.org/10.1016/j.gca.2015.09.017>
- Vats N, Mishra S, Singh RK, Gupta AK, Pandey DK (2020) Paleooceanographic changes in the East China Sea during the last ~ 400 kyr reconstructed using planktic foraminifera. *Global Planet Change* 189:103173. <https://doi.org/10.1016/j.gloplacha.2020.103173>
- Wang L, Sarnthein M, Grootes PM, Erlenkeuser H (1999) Millennial recurrence of century-scale abrupt events of East Asian Monsoon: a possible heat conveyor for the global deglaciation. *Paleoceanography* 14(6):725–731. <https://doi.org/10.1029/1999PA900028>
- Wang Y, Cheng H, Edwards RL, Kong X, Shao X, Chen S, Wu J, Jiang X, Wang X, An Z (2008) Millennial- and orbital-scale changes in the East Asian monsoon over the past 224,000 years. *Nature* 451(7182):1090–1093. <https://doi.org/10.1038/nature06692>
- Wang Z, Chen S, Wang Y, Zhao K, Liang Y, Cheng H, Shao Q, Wang X, Zhang J, Wang Q, Zhai X, Edwards RL (2022) A high-resolution stalagmite record from Luoshui Cave, Central China over the past 235 kyr. *Quatern Sci Rev* 282:107443. <https://doi.org/10.1016/j.quascirev.2022.107443>
- Wei K-Y, Mii H-S, Huang C-Y (2005) Age model and oxygen isotope stratigraphy of Site ODP 1202 in the southern Okinawa Trough, Northwestern Pacific. *TAO Terr Atmos Ocean Sci* 16(1):1
- Wessel P, Luis JF, Uieda LA, Scharroo R, Wobbe F, Smith WH, Tian D (2019) The generic mapping tools version 6. *Geochem Geophys Geosyst* 20(11):5556–5564. <https://doi.org/10.1029/2019GC008515>
- Wu Y, Li T-Y, Yu T-L, Shen C-C, Chen C-J, Zhang J, Li J-Y, Wang T, Huang R, Xiao S-Y (2020) Variation of the Asian summer monsoon since the last glacial-interglacial recorded in a stalagmite from southwest China. *Quatern Sci Rev* 234:106261. <https://doi.org/10.1016/j.quascirev.2020.106261>
- Xu X, Oda M (1999) Surface-water evolution of the eastern East China Sea during the last 36,000 years. *Mar Geol* 156(1):285–304. [https://doi.org/10.1016/S0025-3227\(98\)00183-2](https://doi.org/10.1016/S0025-3227(98)00183-2)
- Yanase W, Abe-Ouchi A (2007) The LGM surface climate and atmospheric circulation over East Asia and the North Pacific in the PMIP2 coupled model simulations. *Clim Past* 3(3):439–451. <https://doi.org/10.5194/cp-3-439-2007>
- Yanase W, Abe-Ouchi A (2010) A numerical study on the atmospheric circulation over the midlatitude North Pacific during the Last Glacial Maximum. *J Clim* 23(1):135–151. <https://doi.org/10.1175/2009JCLI3148.1>
- Yang Y, Xiang R, Zhang L, Zhong F, Zhang M (2020) Is the upward release of intermediate ocean heat content a possible engine for low-latitude processes? *Geology* 48(6):579–583. <https://doi.org/10.1130/G47271.1>
- Yokoyama Y, Lambeck K, De Deckker P, Johnston P, Fifield LK (2000) Timing of the Last Glacial Maximum from observed sea-level minima. *Nature* 406(6797):713–716. <https://doi.org/10.1038/355021035>
- Yokoyama Y, Kido Y, Tada R, Minami I, Finkel RC, Matsuzaki H (2007) Japan Sea oxygen isotope stratigraphy and global sea-level changes for the last 50,000 years recorded in sediment cores from the Oki Ridge. *Paleoceanogr Paleoclimatol Paleoeoccl* 247(1):5–17. <https://doi.org/10.1016/j.palaeo.2006.11.018>. **(Quaternary Paleooceanography of the Japan Sea and its linkage with Asian Monsoon)**
- Yokoyama Y, Esat TM, Thompson WG, Thomas AL, Webster JM, Miyairi Y, Sawada C, Aze T, Matsuzaki H, Okuno J, Fallon S, Braga J-C, Humblet M, Iryu Y, Potts DC, Fujita K, Suzuki A, Kan H (2018) Rapid glaciation and a two-step sea level plunge into the Last Glacial Maximum. *Nature* 559(7715):603. <https://doi.org/10.1038/s41586-018-0335-4>
- Zhang H, Griffiths ML, Huang J, Cai Y, Wang C, Zhang F, Cheng H, Ning Y, Hu C, Xie S (2016) Antarctic link with East Asian summer monsoon variability during the Heinrich Stadial-Bølling interstadial transition. *Earth Planet Sci Lett* 453:243–251. <https://doi.org/10.1016/j.epsl.2016.08.008>

- Zhao D, Wan S, Clift PD, Tada R, Huang J, Yin X, Liao R, Shen X, Shi X, Li A (2018) Provenance, sea-level and monsoon climate controls on silicate weathering of yellow river sediment in the northern Okinawa Trough during late last glaciation. *Palaeogeogr Palaeoclimatol Palaeoecol* 490:227–239. <https://doi.org/10.1016/j.palaeo.2017.11.002>
- Zhu J, Liu Z, Brady E, Otto-Bliesner B, Zhang J, Noone D, Tomas R, Nusbaumer J, Wong T, Jahn A, Tabor C (2017) Reduced ENSO variability at the LGM revealed by an isotope-enabled Earth system model. *Geophys Res Lett* 44(13):6984–6992. <https://doi.org/10.1002/2017GL073406>

### **Publisher's Note**

Springer Nature remains neutral with regard to jurisdictional claims in published maps and institutional affiliations.